FIELD INSTRUMENTATION, TESTING, AND LONG-TERM MONITORING OF HIGH-MAST LIGHTING TOWER NO. 1 AT THE I-35/US18 INTERCHANGE NEAR CLEAR LAKE IN THE STATE OF IOWA PHASE 3

Final Report

September 2009

Prepared for:

Iowa Department of Transportation
Office of Bridges and Structures
800 Lincoln Way
Ames, IA 50010

Technical Contact:

Bruce Brakke
Phone: (515) 239-1165
Fax: (515) 239-1978
Email: Bruce.Brakke@dot.state.iowa.gov

Funding Provided by:

Iowa Highway Research Board
TR-562

Prepared by:

Robert J. Connor, Ph.D Ian C. Hodgson, P.E., S.E.

Table of Contents

1. Background

Following the November 12, 2003 collapse of a 140-foot high-mast lighting tower along I-29 in Sioux City, Iowa, an intensive investigation into the cause of failure was carried out by the late Robert Dexter of the University of Minnesota [1]. Subsequently, two high-mast towers near Clear Lake, Iowa were field-tested and monitored for one year, from October 2004 through November 2005. One of the towers was retrofitted with a steel reinforcing jacket at its base while the other remained as originally designed [2].

An additional phase of testing was undertaken to further study the behavior of the reinforcing jacket and is the subject of this report. Tower No. 1 at the I-35/US 18 interchange located near Clear Lake, Iowa was retrofitted with a steel reinforcing jacket. This reinforcing jacket was designed and installed by Wiss, Janney, Elstner, and Associates. This tower was also tested and monitored in its original as-built condition during the previous study which was reported in 2006 [2].

A photograph of the installation of the reinforcing jacket is presented in Figure 1.1. Static and dynamic load tests were performed and long-term monitoring of the tower was recently completed. This report presents the findings of this third phase of work at this location.

Figure 1.1 – Installation of the reinforcing jacket

1.1 Objectives of the Current Study

The current study was initiated to quantify the stresses induced in critical details on the reinforcing jacket and the tower itself through the use of field instrumentation, load testing, and long-term monitoring.

Strain gages were installed on the both the tower and the reinforcing jacket. Additional strain gages were installed on two anchor rods. Tests were conducted with and without the reinforcing jacket installed. Data were collected from all strain gages during static load testing and were used to study the stress distribution of the tower caused by known loads, both with and without the reinforcing jacket. The tower was tested dynamically by first applying a static load, and then quickly releasing the load causing the tower to vibrate freely.

Furthermore, the tower was monitored over a period of over 1 year to obtain stress range histograms at the critical details to be used for a fatigue evaluation. Also during the long-term monitoring, triggered time-history data were recorded to study the wind loading phenomena that excite the tower.

1.2 Summary of the Field Testing Program

Installation of all sensors and load testing were conducted during the week of June 26, 2006. The tower is located at I-35 near Clear Lake, Iowa. It is denoted tower number 1 of the I-35/US18 interchange. (This tower was termed the *"As-built tower."* in the previous report [2].)

A series of static and dynamic loading tests were conducted. These tests were conducted by statically loading the towers with a cable fixed at one end, and connected to the tower approximately 35 feet above the base. The load was subsequently released rapidly to allow the tower to vibrate freely. These dynamic, or "pluck," tests produced a free decay vibration signature that are used to extract both the natural frequencies and damping characteristics of the high-mast tower.

In addition to the load testing, a long-term monitoring program was conducted to quantify the response of the tower under natural wind loading. Over 1 year of data were collected during this monitoring. During the long-term monitoring period, time-history data are recorded when wind speeds and/or tower stresses exceed predetermined trigger levels. Additionally, stress-range histograms were continuously developed. Furthermore, wind speed and direction were continuously monitored.

2. Instrumentation Plan and Data Acquisition

The following sections describe the sensors and instrumentation plan used during the static/dynamic testing and the long-term monitoring programs. A detailed instrumentation plan can be found in Appendix A.

2.1 Strain Gages

Strain gages were placed at predetermined locations. All strain gages installed in the field were produced by Measurements Group Inc. and were 0.25 inch gage length, model LWK-06-W250B-350. These gages are uniaxial weldable resistance-type strain gages. Weldable-type strain gages were selected due to the ease of installation in a variety of weather conditions. The "welds" are point or spot resistance welds about the size of a pin prick. The probe is powered by a battery and only touches the foil that the strain gage is mounted on by the manufacturer. This fuses the foil to the steel surface. It takes forty or more of these small "welds" to attach the gage to the steel surface. There are no arc strikes or heat affected zones that are discernible. There is no preheat or any other preparation involved other than the preparation of the local metal surface by grinding and then cleaning before the gage is attached to the component with the welding unit. There has never been an instance of adverse behavior associated with the use of weldable strain gages including their installation on extremely brittle material such as A615 Gr75 steel reinforcing bars.

These strain gages are also temperature compensated and perform very well when accurate strain measurements are required over long periods of time (months to years). The gage resistance is 350 ohms and an excitation voltage of 10 volts was used. All gages were protected with a multi-layer weatherproofing system and then sealed with a silicon type compound.

2.2 Accelerometers

Two uniaxial accelerometers were used for the dynamic tests only. The accelerometers were manufactured by PCB Piezotronics, Inc. (model 3701G3FA3G). This accelerometer has a peak measurable acceleration of 3 g.

These accelerometers are termed capacitive (or DC) accelerometers. The primary component of these sensors is an internal capacitor. When subjected to acceleration, the sensor outputs a voltage in direct proportion to the magnitude of the acceleration. They are specifically designed for measuring low-level, low-frequency accelerations, such as those found on a bridge or a high-mast lighting tower.

2.3 Anemometer

An anemometer is used to measure wind speed and direction and is installed atop a 30 foot wooden telephone pole directly adjacent to the high-mast tower. The anemometer (model number 5103) is manufactured by R.M. Young Inc., and is a propeller type anemometer. Both wind speed and wind direction are measured.

2.4 Data Acquisition System

A Campbell Scientific CR9000 data logger was used for the collection of data during all static and dynamic testing, as well as for the long-term monitoring phase. This logger is a high speed, multi-channel 16-bit data acquisition system. The data logger was configured with digital and analog filters to achieve noise-free signals.

The data logger was enclosed in a weather-tight box adjacent to the tower (see Figure 2.1). Remote communications with the data logger were maintained through a satellite internet connection. Data collection was performed automatically. The satellite link was also used to upload new programs as needed. Data were collected and reviewed periodically to assure the integrity of the data.

Figure 2.1 – Weather-tight enclosure adjacent to the high-mast tower used to house the data acquisition and communications equipment

2.5 Instrumentation Plan

A total of 25 strain gages were applied to the tower. Of these, twelve were installed on the existing tower, nine were installed on the reinforcing jacket, and the remaining four gages were installed on two anchor rods. Key drawings are presented in Figure 2.2 and Figure 2.3. Complete details of the instrumentation plan can be found in Appendix A.

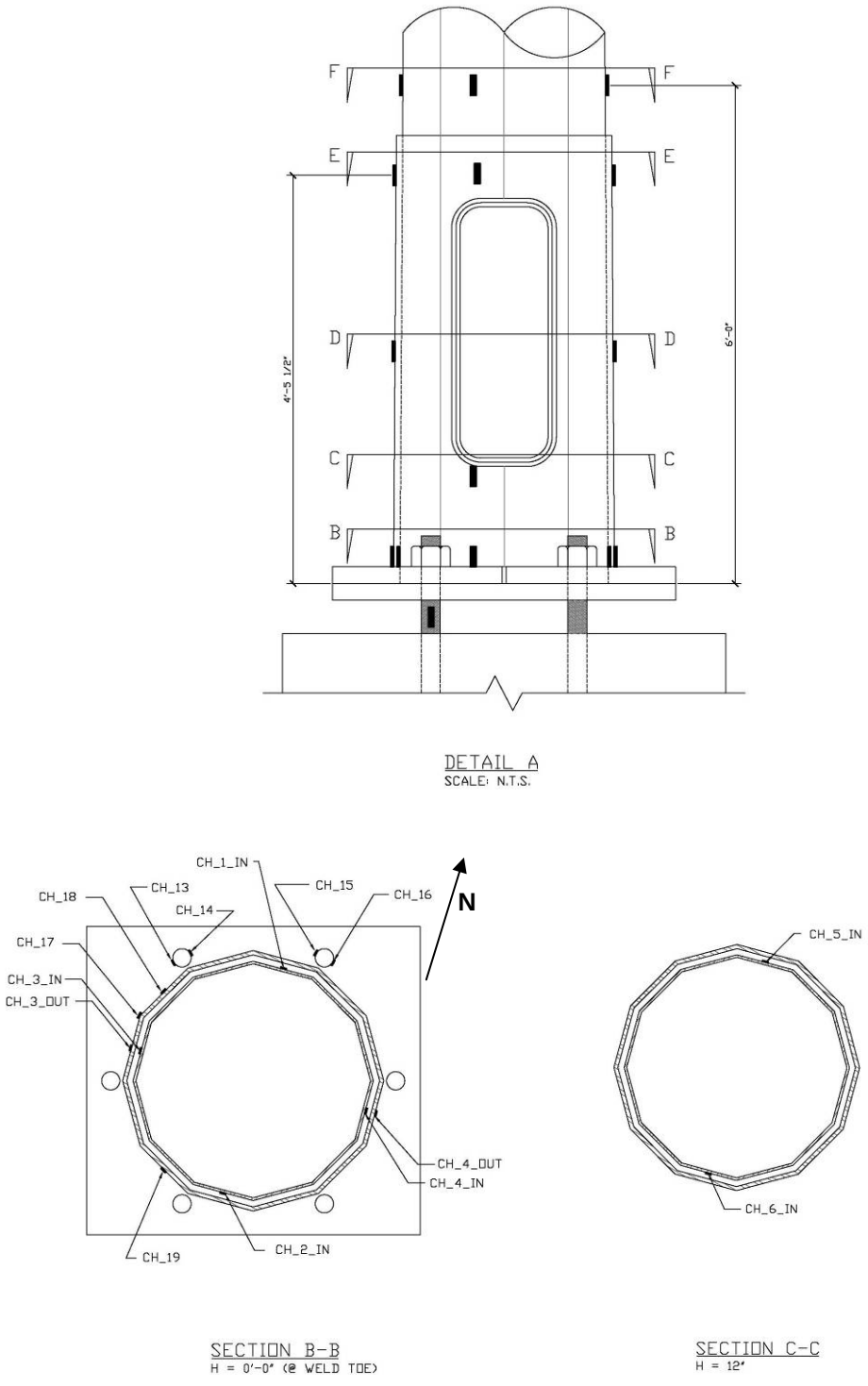

Figure 2.2 – Section drawings showing strain gage locations (part 1/2)

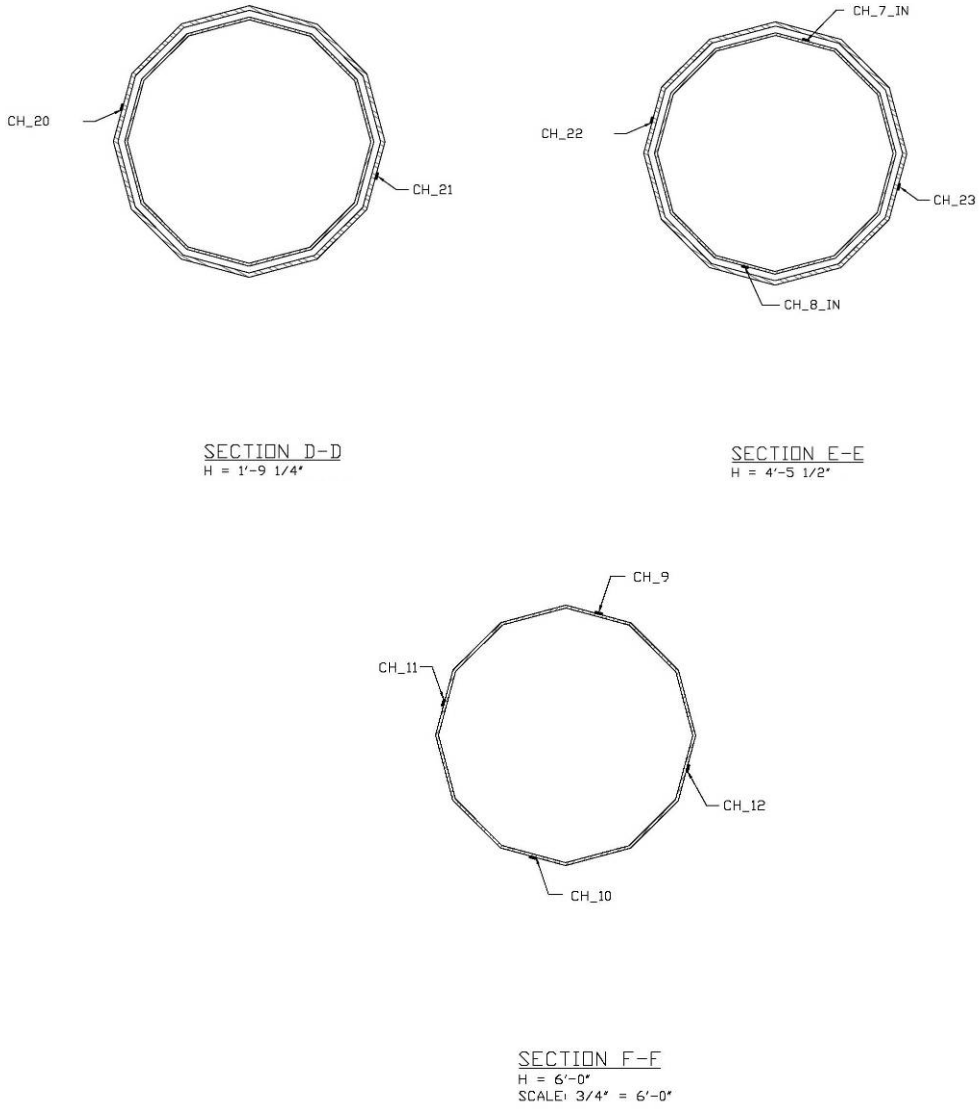

Figure 2.3 – Section drawings showing strain gage locations (part 2/2)

On the existing tower, a set of four strain gages were installed 90 degrees apart at a section 6 feet above the base plate. Two strain gages were placed on the tower 180 degrees apart approximately 53 inches above the baseplate (just below the top of the reinforcing jacket). Two strain gages were placed on the tower 180 degrees apart 12 inches above the baseplate. Finally, a set of four strain gages were installed 90 degrees apart adjacent to the base weld. All of these strain gages were oriented vertically. The inside of the reinforcing jacket was ground out at strain gaged locations so pressure would not be applied to the strain gage after the bolted jacket connection was fully tightened. Shown in Figure 2.4 is a photograph of weldable strain gages installed on the existing high mast tower at the toe of the base weld and 12 inches above the base plate. This photograph was taken prior to the installation of weatherproofing material and reinforcing jacket.

Figure 2.4 – Strain gages installed on the existing high-mast tower at the toe of the base weld and 12 in. above the base plate

On the reinforcing jacket, two strain gages were installed 180 degrees apart approximately 53 inches above the baseplate (just below the top of the reinforcing jacket). Two strain gages were installed 180 degrees apart approximately 21 inches above the baseplate. Finally five strain gages were placed around the perimeter of the reinforcing jacket adjacent to the base weld. Again, all of these strain gages were oriented vertically.

Two anchor rods on the north side of the tower were instrumented. These are shown in Figure 2.5. On each anchor rod, two strain gages were installed 180 degrees apart on the free length of the anchor rod between the concrete foundation and the

underside of the base plate. A view of the completed reinforcing jacket can be seen in Figure 2.6.

Figure 2.5 – Strain gage installed on the anchor rod between the concrete foundation and lower leveling nut

Figure 2.6 – Base of high-mast tower after installation of reinforcing jacket and all instrumentation

3. Results of Static Testing

Static tests were performed on the high-mast tower, both with and without the reinforcing jacket in place. In both cases, the load was applied in both the north and west directions. Tests were repeated multiple times. The load was applied using a nylon sling wrapped around the tower at a height of approximately 35 feet. The load was applied using a come-along connected to the sling with a wire rope. The other end of the wire rope was connected to the back of a heavy truck at ground level. This is shown schematically in Figure 3.1. As a result of the inclination of the cable, a lateral force (causing bending) and a downward force (causing compression) are applied to the tower.

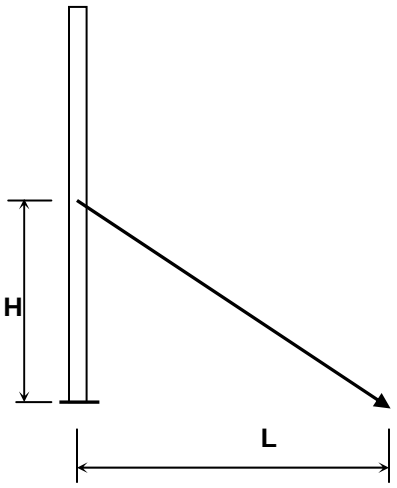

Figure 3.1 – Schematic drawing of static pull tests with key dimensions

Presented in Table 3.1 and Table 3.2 are the peak stresses measured in all strain gages on the as-built tower (no reinforcing jacket) for pull tests in the north-south and east-west directions, respectively. Also shown in the table are the calculated moment and stress at a section 6 feet above the baseplate. This is compared to the measured bending stress, calculated by taking the average of the peak stress measured at the two gages on opposite sides of the tower in line with the load. The measurements from strain gages CH_9, 10, 11, and 12 are used for this calculation. For north-south loading, the bending stress is equal to (CH_10 – CH_9)/2. For east-west loading, the bending stress is equal to (CH_12 – CH_11)/2. It can be seen that there is good agreement between the calculated and measured bending stress.

Table 3.3 and Table 3.4 contain the peak measured stresses in all strain gages on the retrofitted tower (with reinforcing jacket) for the pull tests in the north-south and east-west directions, respectively. Again, it can be seen that there is good agreement between the calculated and measured bending stress. Strain gages CH_7_IN and CH_8_IN failed after installation of the reinforcing jacket.

In the jacket-reinforced tower, it can be seen that at the base of the tower section (CH_1_IN, CH_2_IN, CH_3_IN, and CH_4_IN), significant stress levels remain in the tower, though they are markedly reduced from the as-built case.

Data Channel	Location	NS Pull				Unit
		Pull_1	Pull_2	Pull_3	Pull_4	
CH_1_IN	N face tower at base	-2.60	-3.39	-6.40	-6.07	ksi
CH_2_IN	S face tower at base	2.23	3.28	6.53	6.51	ksi
CH_3_IN	W face tower at base	-0.19	-0.17	0.15	0.05	ksi
CH_4_IN	E face tower at base	-0.09	0.12	-0.12	0.29	ksi
CH_5_IN	N face tower 12" above base	-1.41	-1.74	-3.25	-2.97	ksi
CH_6_IN	S face tower 12" above base	1.24	1.95	3.86	3.89	ksi
CH_7_IN	N face tower 53.5" above base	-1.43	-1.77	-3.35	-3.02	ksi
CH_8_IN	S face tower 53.5" above base	1.16	1.84	3.62	3.75	ksi
CH_13	NW anchor rod	-0.81	-0.98	-1.60	-1.51	ksi
CH_14	NW anchor rod	-1.72	-2.22	-4.01	-3.87	ksi
CH_15	N anchor rod	-1.21	-1.46	-2.83	-2.52	ksi
CH_16	N anchor rod	-2.14	-2.79	-5.39	-5.07	ksi
CH_9	N face tower 6' above base	-1.30	-1.59	-3.09	-2.72	ksi
CH_10	S face tower 6' above base	1.02	1.57	3.13	3.17	ksi
CH_11	W face tower 6' above base	-0.11	-0.07	0.18	0.21	ksi
CH_12	E face tower 6' above base	-0.14	0.09	-0.04	0.27	ksi
Load		0.78	1.06	1.83	2.02	kips
Moment @ 6' above baseplate		19.82	26.82	46.44	51.40	k-ft
Calculated Stress		1.18	1.59	2.76	3.05	ksi
Measured Bending Stress		1.16	1.58	3.11	2.94	ksi
Meas./Calc'd Stress		0.99	0.99	1.13	0.96	ksi

H= 35', L = 63.6'

Table 3.1 – As-built tower – stresses measured during static north-south pull tests

Data Channel	Location	EW Pull		Unit
		Pull_5	Pull_6	
CH_1_IN	N face tower at base	0.26	0.47	ksi
CH_2_IN	S face tower at base	0.36	0.39	ksi
CH_3_IN	W face tower at base	-7.39	-7.19	ksi
CH_4_IN	E face tower at base	7.27	7.35	ksi
CH_5_IN	N face tower 12" above base	0.21	0.42	ksi
CH_6_IN	S face tower 12" above base	0.31	0.28	ksi
CH_7_IN	N face tower 53.5" above base	0.06	0.20	ksi
CH_8_IN	S face tower 53.5" above base	-0.29	-0.23	ksi
CH_13	NW anchor rod	-2.79	-2.69	ksi
CH_14	NW anchor rod	-3.38	-3.19	ksi
CH_15	N anchor rod	1.07	1.28	ksi
CH_16	N anchor rod	1.60	1.76	ksi
CH_9	N face tower 6' above base	0.01	0.21	ksi
CH_10	S face tower 6' above base	0.21	0.19	ksi
CH_11	W face tower 6' above base	-3.07	-2.95	ksi
CH_12	E face tower 6' above base	3.34	3.46	ksi
Load		2.03	2.02	kips
Moment @ 6' above baseplate		52.52	52.20	k-ft
Calculated Stress		3.12	3.10	ksi
Measured Bending Stress		3.20	3.20	ksi
Meas./Calc'd Stress		1.03	1.03	ksi

H= 35', L = 68.4'

Table 3.2 – As-built tower – stresses measured during static east-west pull tests

Data Channel	Location	NS Pull			Units
		Pluck_A	Pluck_B	Pluck_C	
CH_1_IN	N face tower at base	-2.48	-0.99	-1.70	ksi
CH_2_IN	S face tower at base	2.93	4.34	3.05	ksi
CH_3_IN	W face tower at base	0.61	2.01	1.01	ksi
CH_4_IN	E face tower at base	0.49	1.97	1.02	ksi
CH_5_IN	N face tower 12" above base	-0.66	0.76	-0.08	ksi
CH_6_IN	S face tower 12" above base	1.62	3.11	1.99	ksi
CH_13	NW anchor rod	-2.59	-1.01	-1.86	ksi
CH_14	NW anchor rod	-2.56	-1.54	-2.23	ksi
CH_15	N anchor rod	-1.10	0.36	-0.50	ksi
CH_16	N anchor rod	-5.44	-4.39	-4.67	ksi
CH_9	N face tower 6' above base	-2.56	-1.06	-1.93	ksi
CH_10	S face tower 6' above base	3.05	4.92	3.47	ksi
CH_11	W face tower 6' above base	0.53	2.09	1.00	ksi
CH_12	E face tower 6' above base	0.37	2.01	0.97	ksi
CH_3_OUT	W face jacket at base	0.41	1.64	0.70	ksi
CH_4_OUT	E face jacket at base	0.38	1.77	0.90	ksi
CH_17	WNW face jacket at base on bend	-1.26	0.08	-0.87	ksi
CH_18	WNW face jacket at base	-1.22	-0.29	-1.03	ksi
CH_19	SSW face jacket at base	3.11	4.74	3.36	ksi
CH_20	W face jacket 21.25" above base	0.30	1.78	0.69	ksi
CH_21	E face jacket 21.25" above base	0.18	1.46	0.55	ksi
CH_22	W face jacket 53.5" abv base	0.29	1.36	0.59	ksi
CH_23	E face jacket 53.5" abv base	0.36	2.02	0.70	ksi
Load		1.95	1.98	1.89	kips
Moment @ 6' above baseplate		49.56	50.22	47.99	k-ft
Calculated Stress		2.94	2.98	2.85	ksi
Measured Bending Stress		2.81	2.99	2.70	ksi
Meas./Calc'd Stress		0.95	1.00	0.95	ksi

H= 35', L = 63.6'

Table 3.3 – Retrofitted tower – stresses measured during static north-south pull tests

Data Channel	Location	EW Pull		Units
		Pluck_D	Pluck_E	
CH_1_IN	N face tower at base	-0.88	-0.28	ksi
CH_2_IN	S face tower at base	-0.69	-0.36	ksi
CH_3_IN	W face tower at base	-3.68	-2.52	ksi
CH_4_IN	E face tower at base	2.40	2.32	ksi
CH_5_IN	N face tower 12" above base	-0.98	-0.44	ksi
CH_6_IN	S face tower 12" above base	-0.53	-0.17	ksi
CH_13	NW anchor rod	-3.93	-2.80	ksi
CH_14	NW anchor rod	-4.43	-3.27	ksi
CH_15	N anchor rod	-0.34	0.06	ksi
CH_16	N anchor rod	-0.26	0.43	ksi
CH_9	N face tower 6' above base	-1.46	-0.75	ksi
CH_10	S face tower 6' above base	-0.85	-0.56	ksi
CH_11	W face tower 6' above base	-3.79	-2.82	ksi
CH_12	E face tower 6' above base	2.07	2.05	ksi
CH_3_OUT	W face jacket at base	-3.39	-2.67	ksi
CH_4_OUT	E face jacket at base	2.40	2.32	ksi
CH_17	WNW face jacket at base on bend	-6.51	-5.09	ksi
CH_18	WNW face jacket at base	-3.86	-2.87	ksi
CH_19	SSW face jacket at base	-1.84	-1.41	ksi
CH_20	W face jacket 21.25" above base	-1.96	-1.37	ksi
CH_21	E face jacket 21.25" above base	0.38	0.59	ksi
CH_22	W face jacket 53.5" abv base	-1.72	-1.22	ksi
CH_23	E face jacket 53.5" abv base	0.33	0.54	ksi
Load		1.94	1.68	kips
Moment @ 6' above baseplate		50.04	43.38	k-ft
Calculated Stress		2.97	2.57	ksi
Measured Bending Stress		2.93	2.44	ksi
Meas./Calc'd Stress		0.99	0.95	ksi

H= 35', L = 68.4'

Table 3.4 – Retrofitted tower – stresses measured during static east-west pull tests

4. Results of Long-Term Monitoring

Stress-range histograms were developed continuously for all strain gages throughout all phases of monitoring. Every ten minutes, histograms were updated for each strain gage and written to a file. The rainflow cycle-counting algorithm was used to develop the stress-range histograms [3]. This algorithm matches up peaks in the random variable response to define individual cycles, and then organizes these stress-range cycles into bins to create a histogram. The stress range histogram is essentially a bar graph with 0.5 ksi stress-range bins (i.e., 0-0.5, 0.5-1.0, etc.). In any particular bin, the histogram contains the number of stress cycles that were measured whose magnitudes fall within that bin.

A fatigue evaluation of the tower was performed using the stress-range histograms, which were truncated at a level equal to approximately 1/4 of the constant amplitude fatigue limit (CAFL) of the detail in question per AASHTO. That is, all cycles with stress ranges less than the truncation level were removed from the histogram prior to calculation of the effective stress. An in-depth discussion of the methodology used for the fatigue evaluation can be found in Appendix B.

In addition to the stress-range histograms, stress time-history data were recorded when predefined trigger events occurred. These "trigger events" occurred when wind speed and stress events at selected locations exceeded various levels. When a trigger event was detected, data were recorded from all sensors for a predefined length of time. The stress time history data were used to assess the validity of large stress-range cycles recorded in the stress-range histograms, and to understand the wind phenomena that caused them. Two types of trigger events were considered. First, data were recorded based on wind speed. When the wind speed exceeded 15, 30, and 45 mph, data were recorded to corresponding data files. Second, when the stress in the pole wall above the jacket exceeded a given threshold, time-history data were recorded. Two directions of pole loading were considered.

Finally, average wind data were recorded continuously, on five minute intervals. During each interval, the data logger recorded the average wind direction, as well as the maximum wind speed and the average wind speed.

4.1 Stress-Range Histograms

A total of ten strain gages were monitored as identified in Table 4.1. Figure 4.1, Figure 4.2, and Table 4.2 contain the measured stress-range histograms for these ten strain gages for the period between November 8, 2006 through July 31, 2008. Data were not recorded continuously due to various outages. During this period, a total of 380 days of data were collected. Strain gage CH_16 failed during the monitoring period and therefore only 290 days of data were obtained. Strain gage CH_19 also failed prematurely and only 53 days of data were obtained. The histograms for CH_16 and CH_19 presented graphically in Figure 4.2 have been scaled up to represent 380 days so direct comparison between all the strain gages can be made. The histograms presented in Table 4.2 are the raw histograms (i.e., not scaled).

Based on these measured histograms and utilizing the AASHTO design S-N curves, a fatigue life estimate was developed for each of the gages listed in Table 4.1, the results of which are presented in Table 4.3.

Strain Gage	Location
CH_1	N side on tower; at base weld centered on face
CH_3IN	W side on tower; at base weld centered on face
CH_3OUT	W side on jacket; at base weld centered on face
CH_9	N side on tower; 6' above baseplate centered on face
CH_11	W side on tower; 6' above baseplate centered on face
CH_14	NW anchor rod
CH_16	N anchor rod
CH_17	W side on jacket; at base weld on bend
CH_19	Base of jacket centered on the SSW face
CH_23	E side on jacket, 4'-5 ½" above baseplate

Table 4.1 – Summary of strain gages for which stress-range histograms were developed

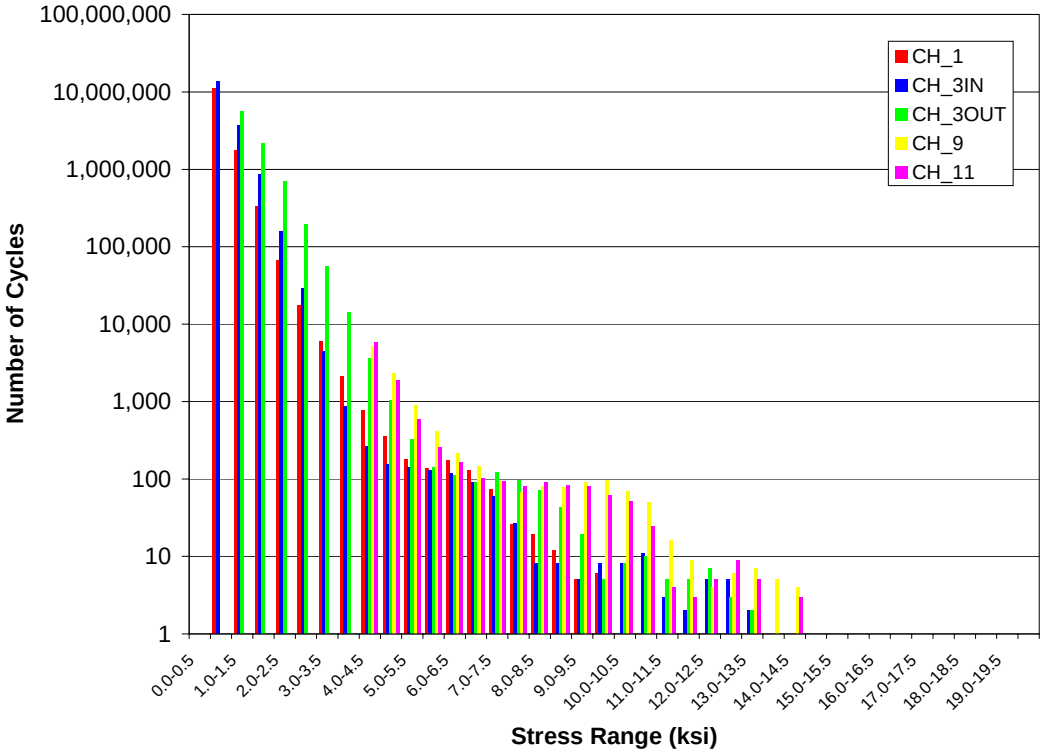

Figure 4.1 – Stress-range histograms 1 - November 8, 2006 through July 31, 2008 total of 380 days of monitoring

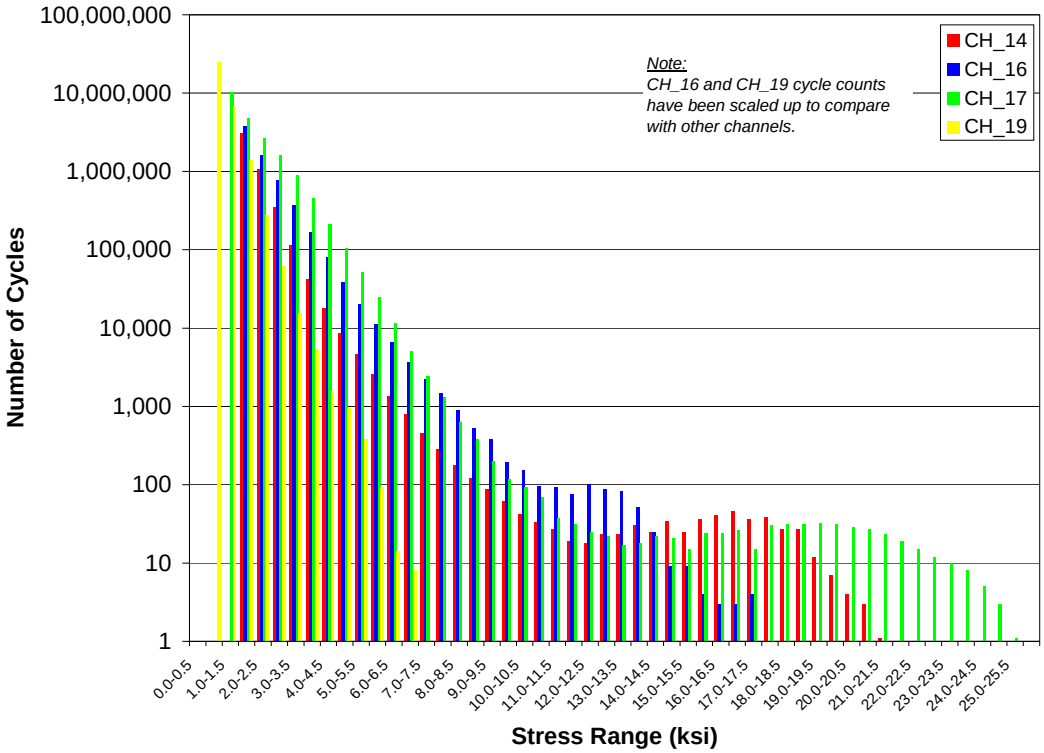

Figure 4.2 – Stress-range histograms 2 - November 8, 2006 through July 31, 2008 total of 380 days of monitoring (except CH_16 and CH_19)

Min (ksi)	Max (ksi)	Avg. (ksi)	CH_1	CH_3IN	CH_3OUT	CH_9	CH_11	CH_14	CH_16	CH_17	CH_19
0.0	0.5	0.25	0	0	0	0	0	0	0	0	0
0.5	1.0	0.75	11,074,846	13,814,015	0	0	0	0	0	0	3,379,409
1.0	1.5	1.25	1,772,466	3,692,103	5,544,070	0	0	0	0	10,383,993	936,532
1.5	2.0	1.75	333,932	847,237	2,179,398	0	0	3,090,698	2,899,217	4,827,099	190,510
2.0	2.5	2.25	66,724	157,473	701,129	0	0	1,078,879	1,240,158	2,685,555	38,328
2.5	3.0	2.75	17,722	29,273	196,217	0	0	354,714	583,223	1,598,558	8,643
3.0	3.5	3.25	5,989	4,461	56,307	0	0	113,675	281,253	906,327	2,116
3.5	4.0	3.75	2,138	863	14,349	0	0	41,821	128,394	452,388	740
4.0	4.5	4.25	759	262	3,579	5,161	5,898	18,072	61,395	210,745	215
4.5	5.0	4.75	351	155	1,027	2,316	1,869	8,649	29,756	105,452	131
5.0	5.5	5.25	178	140	328	893	590	4,583	15,392	52,175	52
5.5	6.0	5.75	136	129	142	405	259	2,580	8,681	25,040	13
6.0	6.5	6.25	172	117	112	218	164	1,354	5,086	11,512	2
6.5	7.0	6.75	130	91	90	145	102	798	2,789	5,042	1
7.0	7.5	7.25	74	59	121	93	93	456	1,701	2,400	0
7.5	8.0	7.75	26	27	96	67	80	282	1,121	1,299	0
8.0	8.5	8.25	19	8	71	81	90	178	680	624	0
8.5	9.0	8.75	12	8	43	77	84	122	405	384	0
9.0	9.5	9.25	5	5	19	89	81	87	292	200	0
9.5	10.0	9.75	6	8	5	97	61	62	148	119	0
10.0	10.5	10.25	0	8	8	70	51	42	116	93	0
10.5	11.0	10.75	0	11	10	49	24	33	73	69	0
11.0	11.5	11.25	0	3	5	16	4	27	70	37	0
11.5	12.0	11.75	0	2	5	9	3	19	58	31	0
12.0	12.5	12.25	0	5	7	4	5	18	78	25	0
12.5	13.0	12.75	0	5	3	6	9	23	68	22	0
13.0	13.5	13.25	0	2	2	7	5	23	63	17	0
13.5	14.0	13.75	0	0	0	5	1	30	40	18	0
14.0	14.5	14.25	0	0	0	4	3	25	19	22	0
14.5	15.0	14.75	0	0	0	0	0	34	7	21	0
15.0	15.5	15.25	0	0	0	0	0	25	7	15	0
15.5	16.0	15.75	0	0	0	0	0	36	3	24	0
16.0	16.5	16.25	0	0	0	0	0	41	2	24	0
16.5	17.0	16.75	0	0	0	0	0	46	2	26	0
17.0	17.5	17.25	0	0	0	0	0	36	3	15	0
17.5	18.0	17.75	0	0	0	0	0	39	0	30	0
18.0	18.5	18.25	0	0	0	0	0	27	0	31	0
18.5	19.0	18.75	0	0	0	0	0	27	0	31	0
19.0	19.5	19.25	0	0	0	0	0	12	0	32	0
19.5	∞	-	0	0	0	0	0	15	0	183	0
		Total number of cycles =	13,275,685	18,546,470	8,697,143	9,812	9,476	4,717,588	5,260,300	21,269,678	4,556,692
		Cycles/day =	34,964	48,846	22,906	26	25	12,425	18,163	56,018	87,001
		S_{Reff} (ksi) =	0.96	1.03	1.64	5.36	5.16	2.18	2.43	2.16	1.03
		S_{Rmax} (ksi)=	10.0	13.5	24.0	14.5	14.5	21.5	17.5	25.5	7.0

Table 4.2 – Stress range histogram for monitoring period between November 8, 2006 and July 31, 2008 (stresses in ksi)

Strain Gage	Assumed Category (CAFL)	S_{Rmax} [1] (ksi)	Cycles > CAFL		S_{Reff} (ksi)	Cycles/ day	Remaining Life (years)	Adjusted Remaining Life (years) Based on Lab Data
			No. Cycles	% Of Total				
CH_1	E' (2.6)	10.0	27,717	0.21%	1.0	34,964	27	162
CH_3IN	E' (2.6)	13.5	35,642	0.19%	1.0	48,846	12	72
CH_3OUT	E (4.5)	13.5	2,094	0.02%	1.6	22,906	30	180
CH_9	B (16)	14.5	0	0.00%	5.4	26	infinite	infinite
CH_11	B (16)	14.5	0	0.00%	5.2	25	infinite	infinite
CH_14	D (7)	21.6[1]	1,757	0.04%	2.2	12,425	39	N/A
CH_16	D (7)	17.5	4,956	0.09%	2.4	13,854	22	N/A
CH_17	E (4.5)	25.8[1]	204,861	0.96%	2.2	56,018	5	30[2]
CH_19	E (4.5)	7.0	199	0.00%	1.0	12,001	infinite	infinite
CH_23	B (16)	5.0	0	0.00%	4.5	1	infinite	infinite

Notes: 1. Maximum stress cycle determined from review of time-history data
2. Estimate of 30 years is conservative.

Table 4.3 – Summary of fatigue life calculations
(November 8, 2006 through July 31, 2008)

The strain gages on the tower beneath the reinforcing jacket adjacent to the full penetration groove weld (strain gages CH_1 and CH_3IN) are considered Category E' due to the fact that the backing bar is not welded to the base plate by a full penetration weld. The strain gages on the reinforcing jacket adjacent to the base weld (CH_3OUT, CH_17, and CH_19) are considered Category E as a full penetration groove weld. The strain gages on the anchor rods (CH_14 and CH_16) are considered Category D. Strain gage CH_23 on the reinforcing jacket some distance above the baseplate is considered Category B as a bolted connection. Strain gages above the jacket on the tower (CH_9 and CH_11) are also considered Category B as a bolted connection.

Note that in Figure 4.1, Figure 4.2, and Table 4.2, very high stress cycles were recorded in a number of the strain gages, in particular gages CH_14 and CH_16 on the anchor rods and CH_17 at the bend line on the west face of the reinforcing jacket. The effect of these higher stress cycles are reflected in the relatively low fatigue life estimates presented in Table 4.3. However it should be noted that the strain gages at the base were installed adjacent to the weld to at the baseplate weld *(in the previous field testing program, the gages were installed 3 inches above)*. As a result, the strain gages in their current position are located in an area of high stress gradient and the measured stresses cannot be directly compared to the earlier phases of testing [2]. **Since the AASHTO S-N curves are calibrated to be used with nominal stresses, the life estimates presented in Table 4.3 are misleading and inaccurate as they underestimate the actual fatigue life.**

As part of another research project recently completed for the Iowa DOT at Purdue University, the fatigue resistance of the bolted retrofit jacket was evaluated. For those tests, additional data were collected regarding the stress profiles near the weld toe and the relationship to the nominal stresses in the jacket was established. Based on that

testing it was found that the stress ranges immediately adjacent to the weld toe were nearly three times greater than the nominal stresses in the jacket. However, the life of the poles in the field can be directly estimated using the field measured data at the base plate weld and comparing to the stress range that the laboratory test was run at the same location. For example, considering channel CH_17, which has the lowest estimated fatigue life, the measured effective stress range is 2.2 ksi. During the laboratory testing, the measured stress range at the same location averaged about 30 ksi and the test ran for 241,650 cycles. Taking the ratio of these two stress range values cubed, one can estimate the life that the laboratory test would be expected to run had the test been run at the lower value of 2.2 ksi. This yields $(30 \text{ ksi} / 2.2 \text{ ksi})^3 = 2535$. The worst test results observed in the laboratory were from retrofit specimen #1, which only lasted 241,650 cycles [9]. The life of the pole in the field can be estimated to be 241,650 cycles x 2535 = 612,582,750 cycles. As shown in Table 4.3, at 56,014 cycles per day, this results in an estimated life of about 30 years. It should also be noted that in the field, the gages were placed immediately adjacent to the weld toe where as those installed in the lab were not as close. Hence, the estimate above for Channel CH_17 (i.e., 30 years) is actually conservative and is likely greater. The last column in Table 4.3 provides the revised estimated fatigue lives based on the results of the laboratory testing.

4.2 Long-Term Wind Data

4.2.1 Summary

Wind data were collected simultaneously with the stress range histogram data. During triggered time-history events, continuous wind speed and direction data were recorded. In addition, average wind speed, maximum wind speed, and average direction were recorded every five minutes for the duration of the monitoring.

Figure 4.3 shows a polar histogram plot for all data collected during the long term monitoring. This plot shows the percent occurrence of winds from all directions in polar form, with zero degrees representing north. It can be seen that the plot has two lobes, indicating that most of the time the wind blows from either the northwest or southeast. The shape of this plot is similar to that developed during the earlier phases of field testing conducted in 2005 [2].

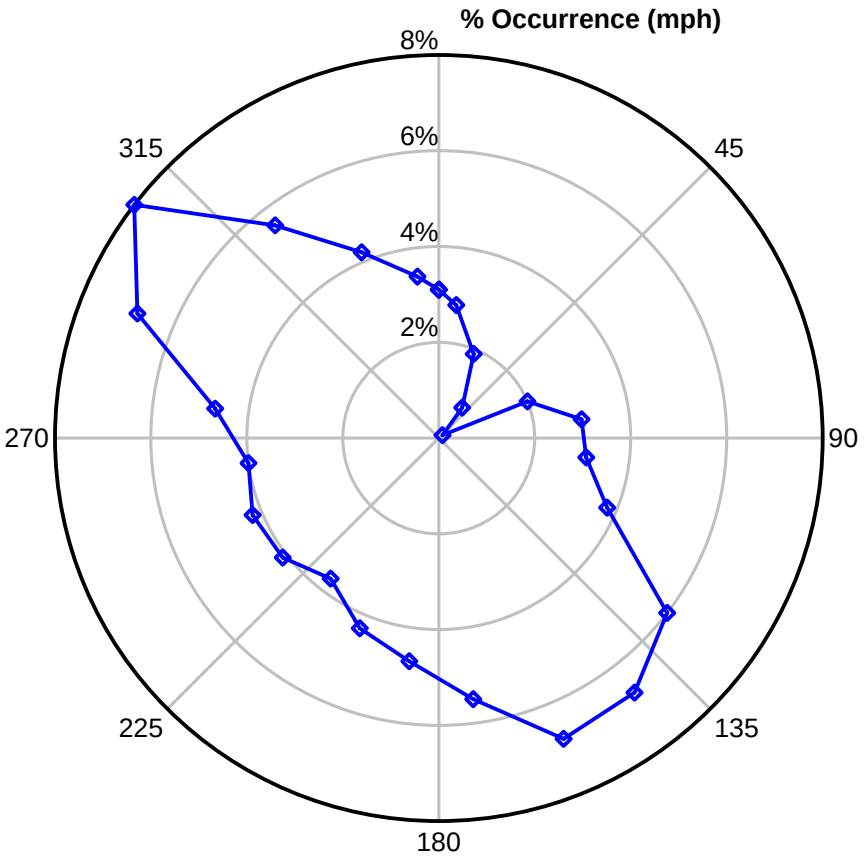

Figure 4.3 – Wind rose for percent occurrence

Figure 4.4 presents a polar histogram plot of average wind speeds, which shows the average wind speed at each direction for the duration of the monitoring period. It can be seen that the highest average wind speeds are approximately 11 mph and generally occur from the same direction (NW) as the most frequent winds, as shown in Figure 4.3.

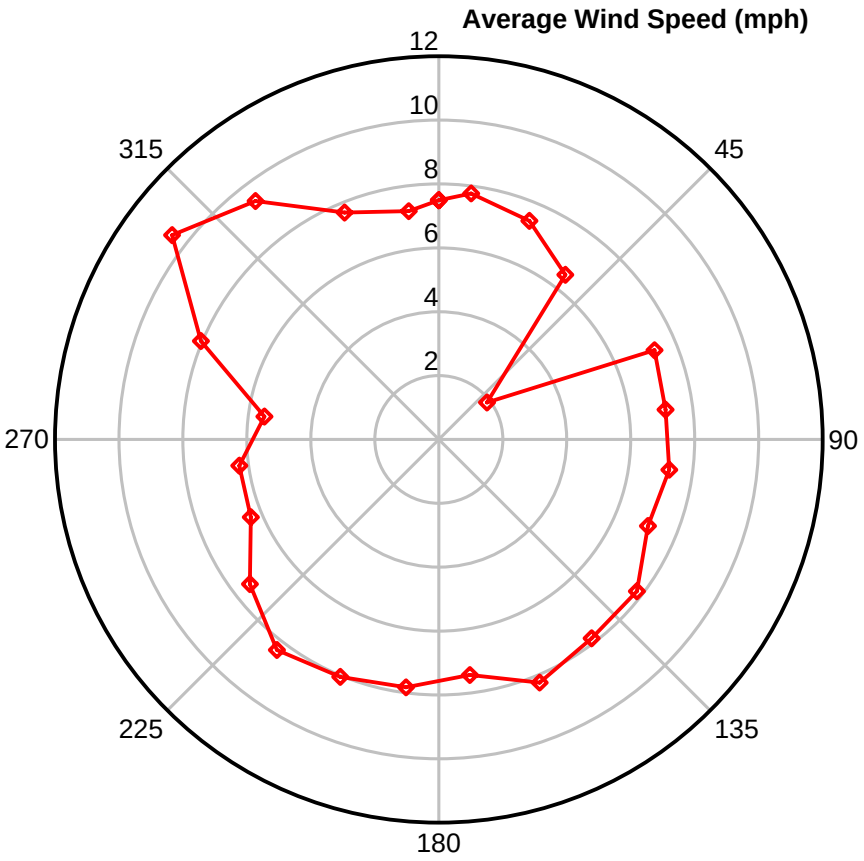

Figure 4.4 – Wind rose of average wind speed

A plot of the average and peak daily wind speeds for the Clear Lake high mast tower is shown in Figure 4.5. It can be seen that the peak wind speed recorded during the monitoring period was 57 mph recorded on July 16, 2007. It is also noted that the wind speed regularly exceeds 30 mph.

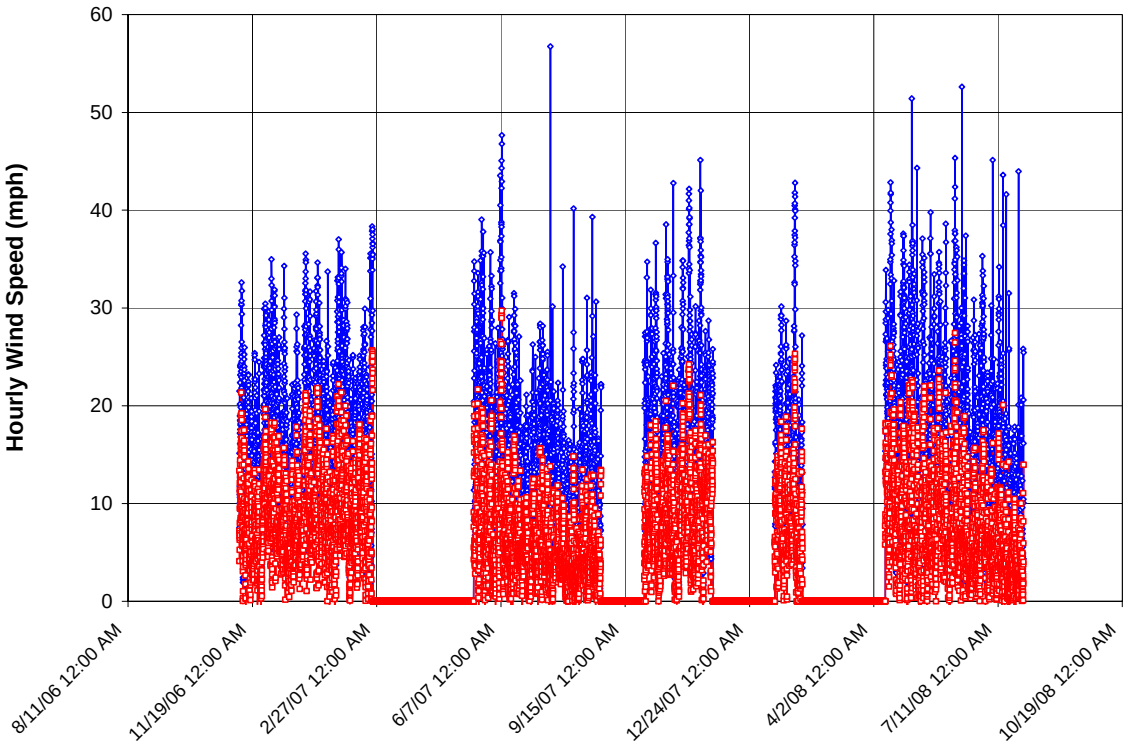

Figure 4.5 - Wind speed history for Clear Lake high mast tower (blue denotes maximum hourly wind speed; red denotes average hourly wind speed)

4.2.2 Natural Wind Gusting

Some of the highest stress cycles recorded during the monitoring period were the result of a wind storm which occurred on November 10, 2006 at approximately 7:10 AM. The average wind speed at the time was only approximately 20 mph with gusts up to 33 mph. This is a very typical range of maximum daily windspeeds as shown in Figure 4.5. The winds were from the north. The stress cycles resulting from this wind event caused a second peak in the stress range histograms at many strain gaged locations as shown in Figure 4.1 and Figure 4.2.

Figure 4.6 through Figure 4.9 present time history-data for all strain gages for this wind event. Also shown in Figure 4.6 are the wind speed and direction. As can be seen, there are large stress range cycles measured at most strain gages. It appears that the tower is excited by an initial gust (see Figure 4.6) that caused the tower to begin vibrating in its first mode. The first mode frequency for this pole is approximately 0.3 Hz (or a period of vibration of 3.3 seconds). This means that the time it takes for the pole to start at a positive peak stress, vibrate to peak negative stress, and return to peak positive stress is 3.3 seconds.

This observed vibration is not vortex shedding since the critical velocity for vortex shedding in the first mode is significantly less than the observed 20 mph present during the event. The wind gusts appear to have been in phase with the first mode natural frequency of the tower, causing the magnitude of vibration to increase.

Figure 4.10 contains a close-up stress time-history for the four strain gages on the tower above the reinforcing jacket (6 feet above the base plate). It can be seen that the time it takes the stress to vary from peak positive to peak negative and back to peak positive stress is approximately 3 seconds. Furthermore, strain gages CH_9 and CH_11 are in phase. Strain gages CH_10 and CH_12 are also in phase with each other, but collectively out-of-phase by 180 degrees with CH_9 and CH_11. Note that the magnitudes are roughly equal. This indicates that the neutral axis of bending lies on a 45 degree line running between CH_9 and CH_11 on one side and CH_10 and CH_12 on the other (i.e., running northeast-southwest).

A similar plot for the four gages on the tower at the base weld (beneath the reinforcing jacket) is shown in Figure 4.11. It can be seen that the same direction of bending is causing the measured stresses.

Large stress ranges were induced in the tower during a large wind gust event that occurred on May 2, 2008. Figure 4.12 presents stress time-history plots for four strain gages, namely CH_9 and 11 (located above the jacket on the north and west faces of the tower, respectively), CH_14 (located on an anchor rod), and CH_17 (located on the west face of the reinforcing jacket at its base on the bend line). Also shown in the plot are the wind speed and direction. The wind reached a peak velocity of over 50 miles per hour and was sustained for a few seconds. This induced large oscillations in the tower. A peak stress range of just over 25 ksi was measured at CH_17.

As noted above, the highest wind speed of 57 mph measured during the monitoring occurred on July 16, 2007. Figure 4.13 presents the time history plots for the same gages as Figure 4.12 during this event. It can be seen that though the wind speed

was higher, the stresses measured during this event were lower than those measured on May 2, 2008 (see Figure 4.12).

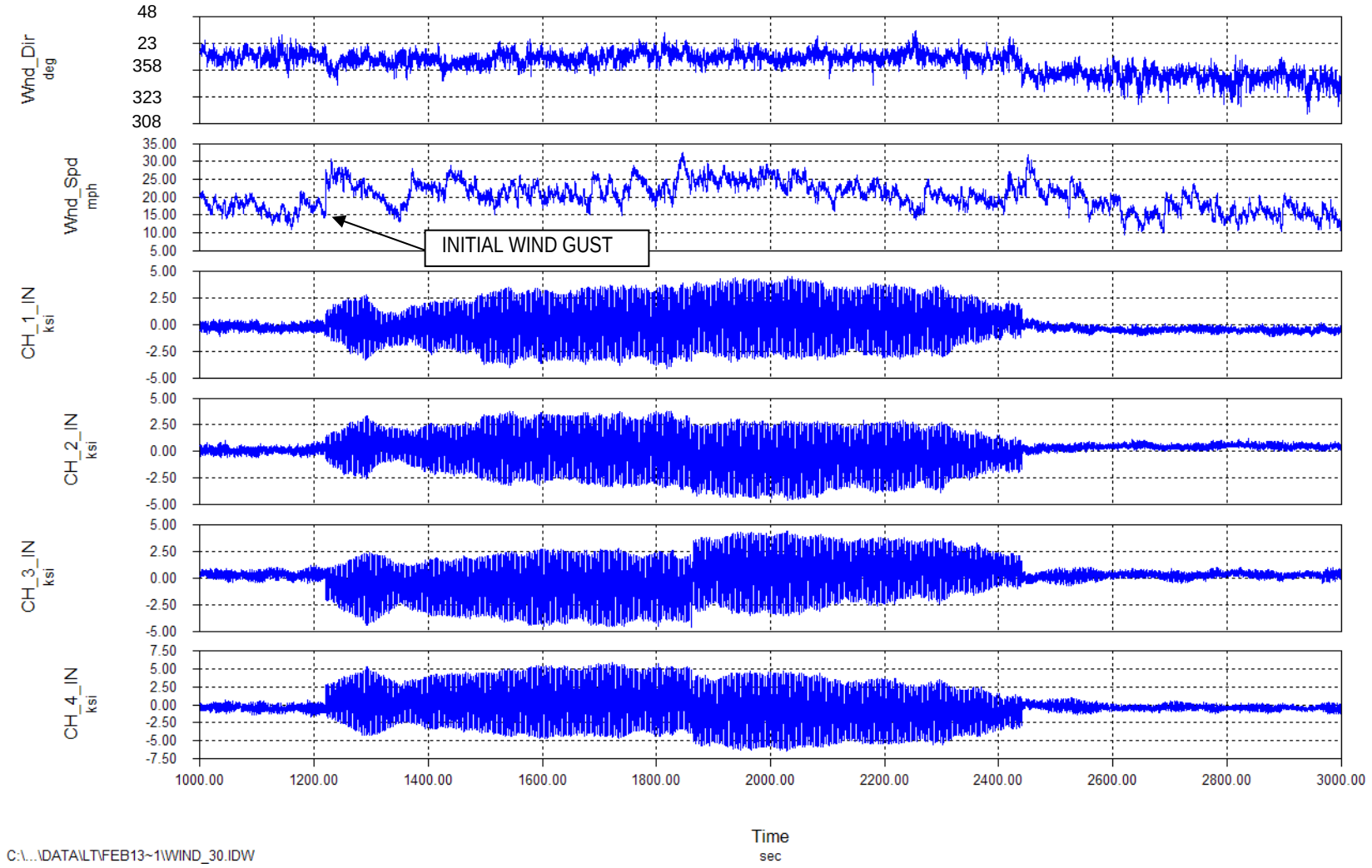

Figure 4.6 – High stress event – November 10, 2006 7:10 AM

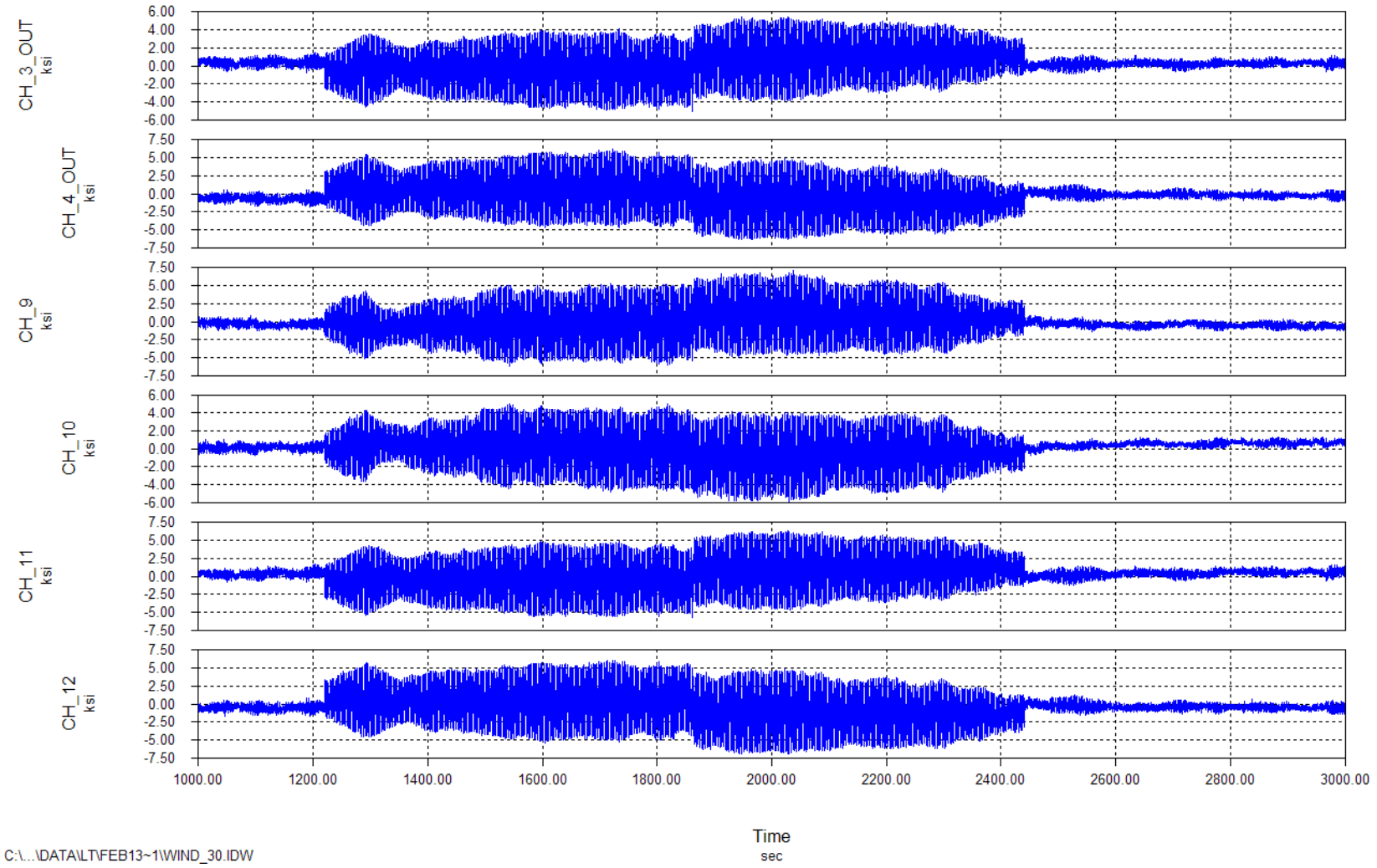

Figure 4.7 – High stress event – November 10, 2006 7:10 AM

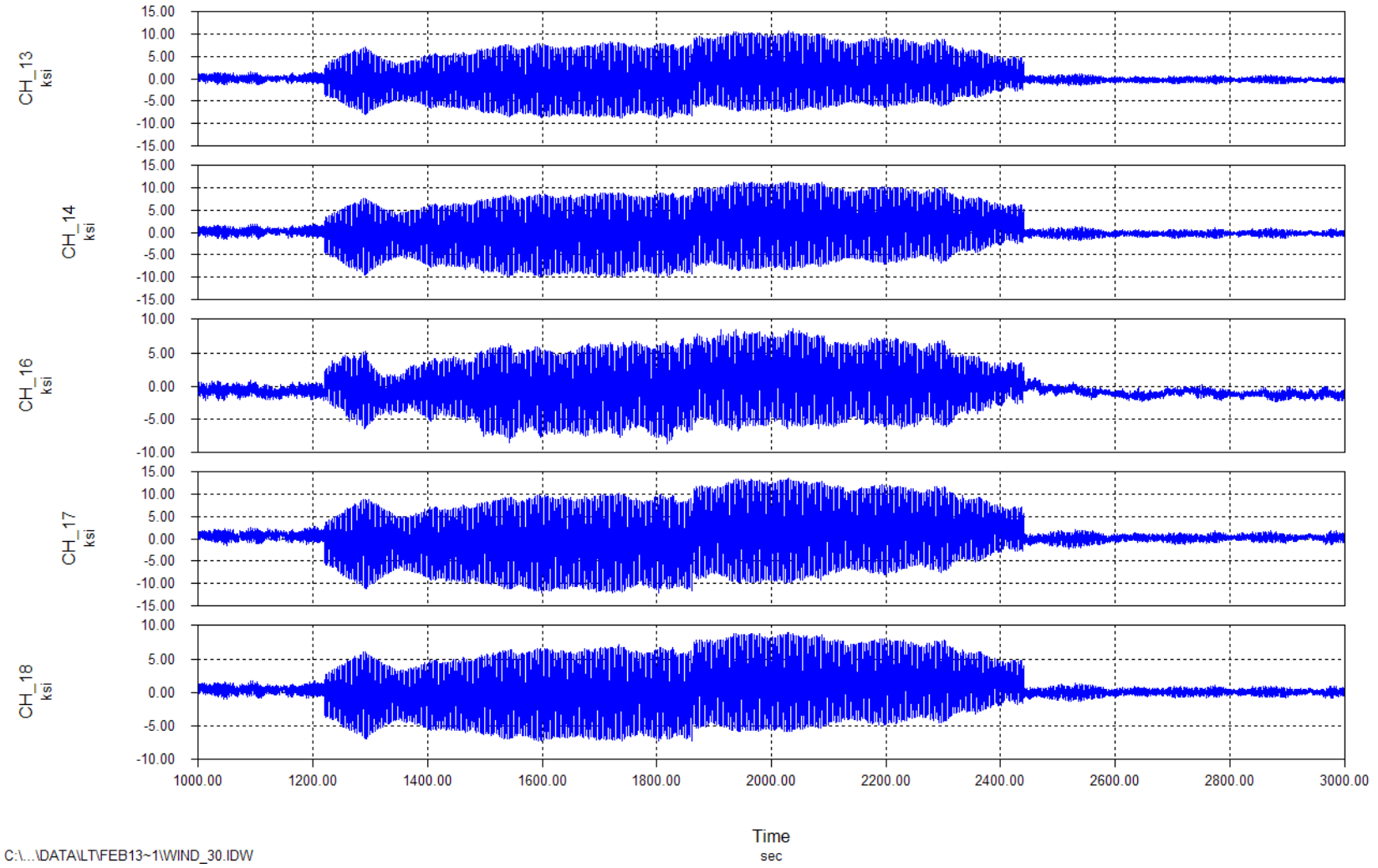

Figure 4.8 – High stress event – November 10, 2006 7:10 AM

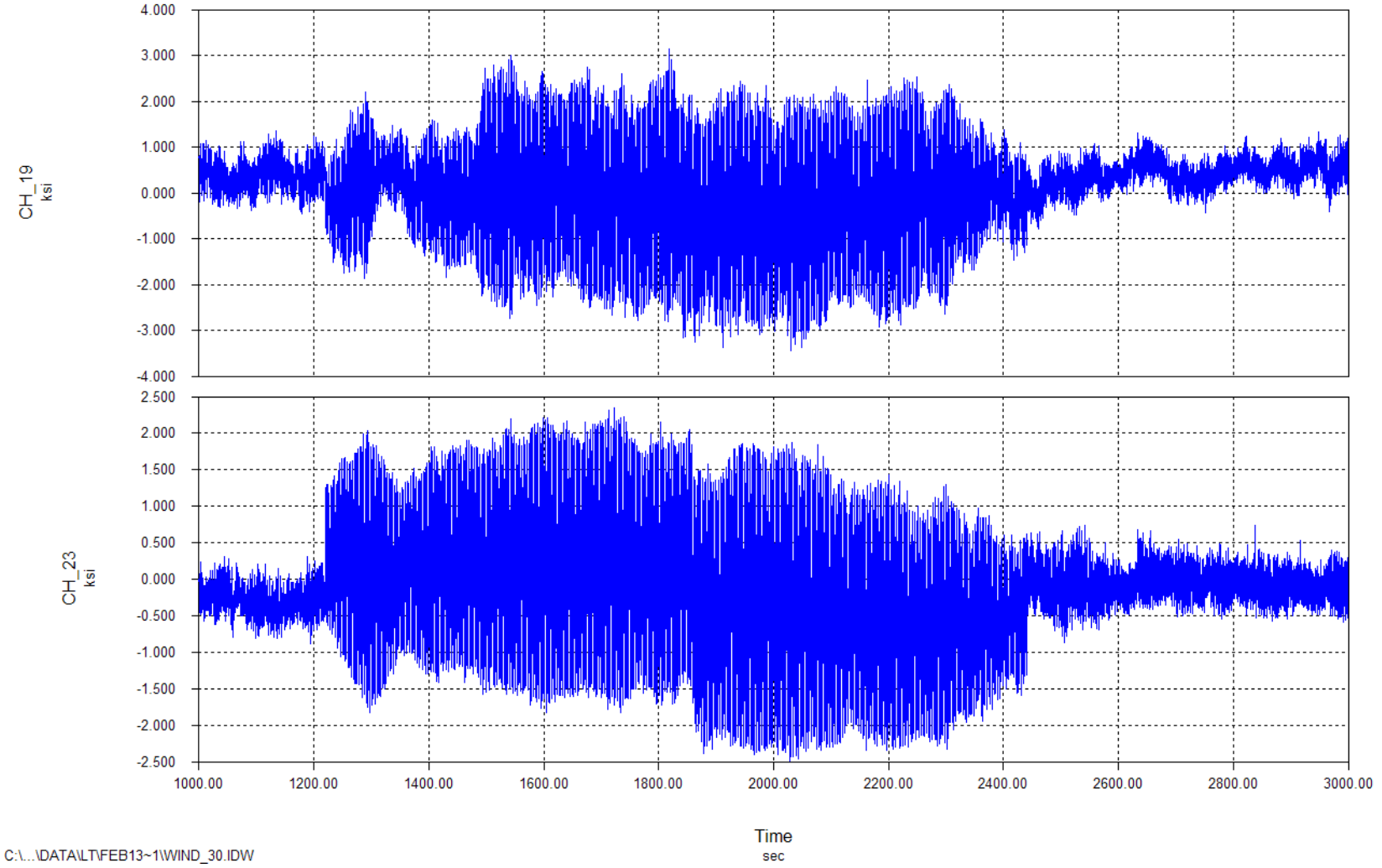

Figure 4.9 – High stress event – November 10, 2006 7:10 AM

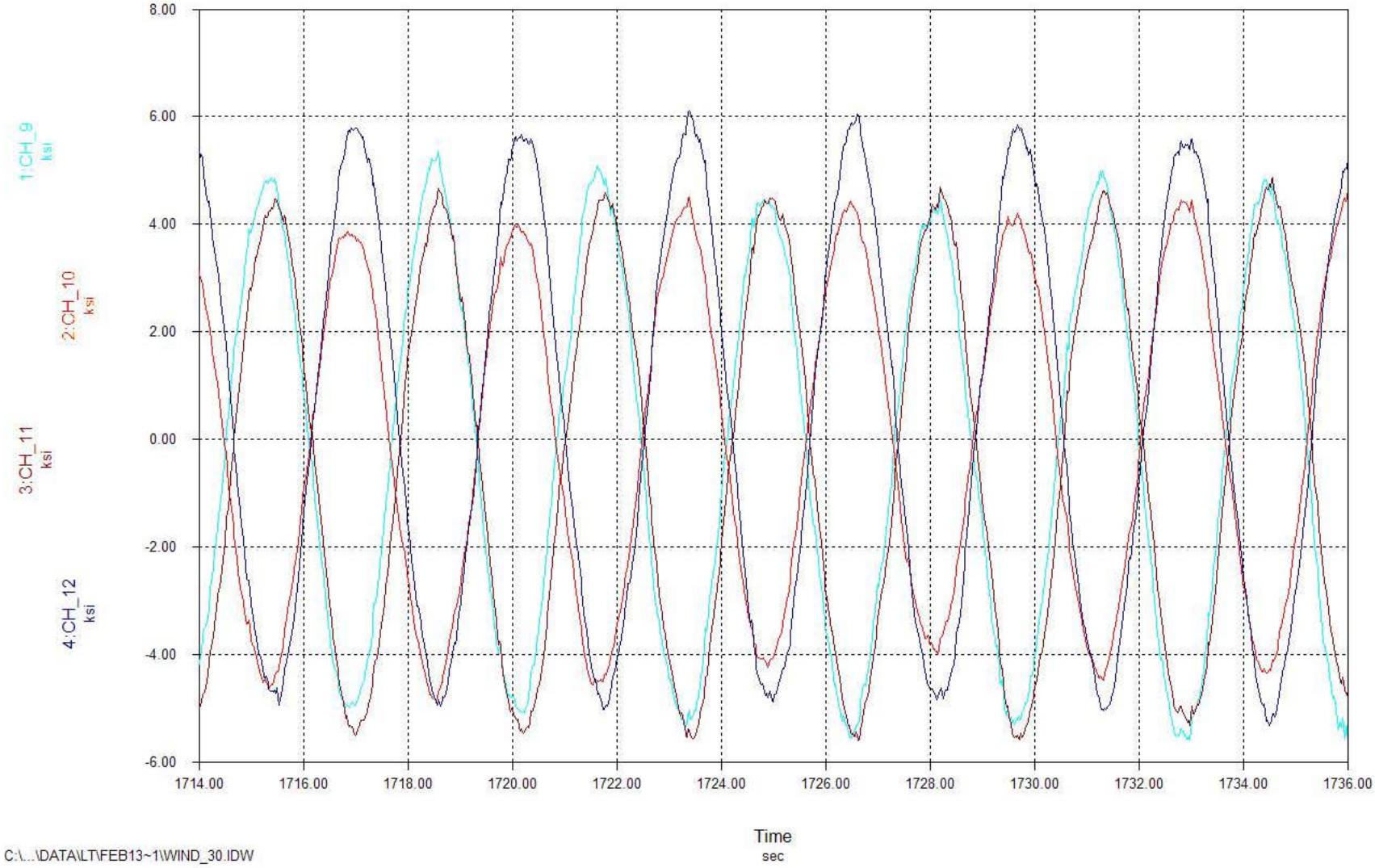

Figure 4.10 – High stress event – November 10, 2006 7:10 AM
Strain gages 6 feet above the baseplate

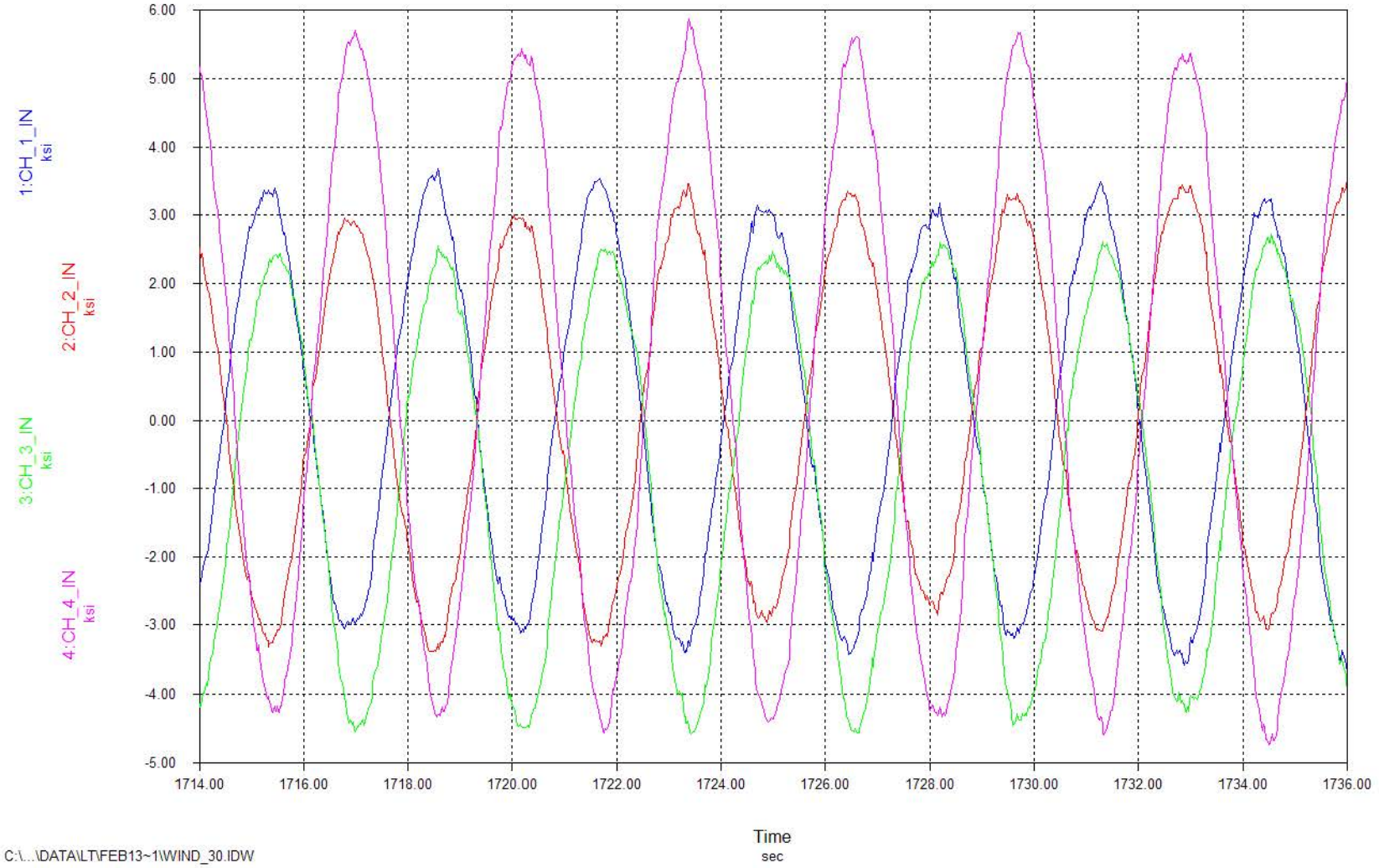

Figure 4.11 – High stress event – November 10, 2006 7:10 AM
Strain gages on the tower at the base weld

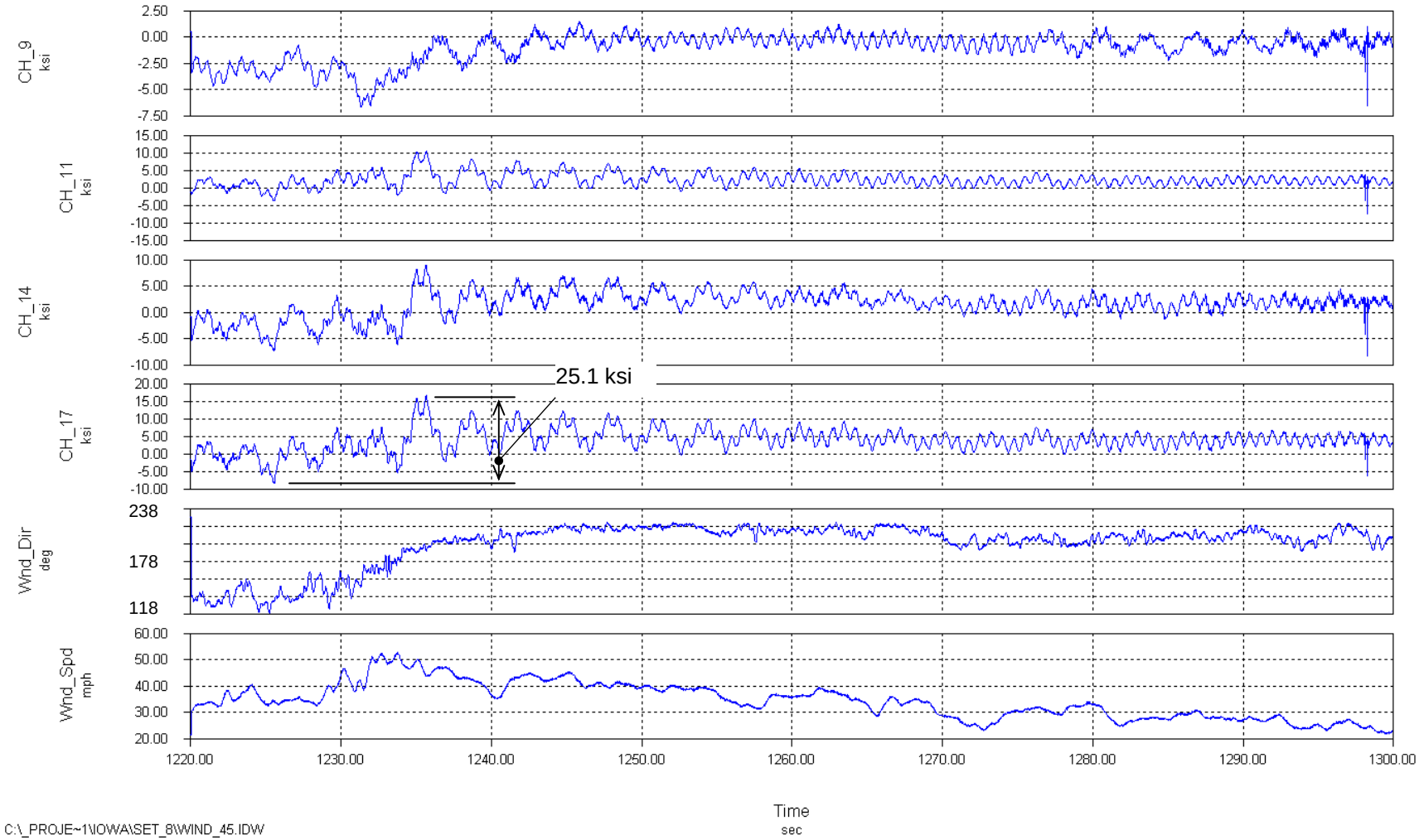

Figure 4.12 – High stress event – May 2, 2008 2:05 PM

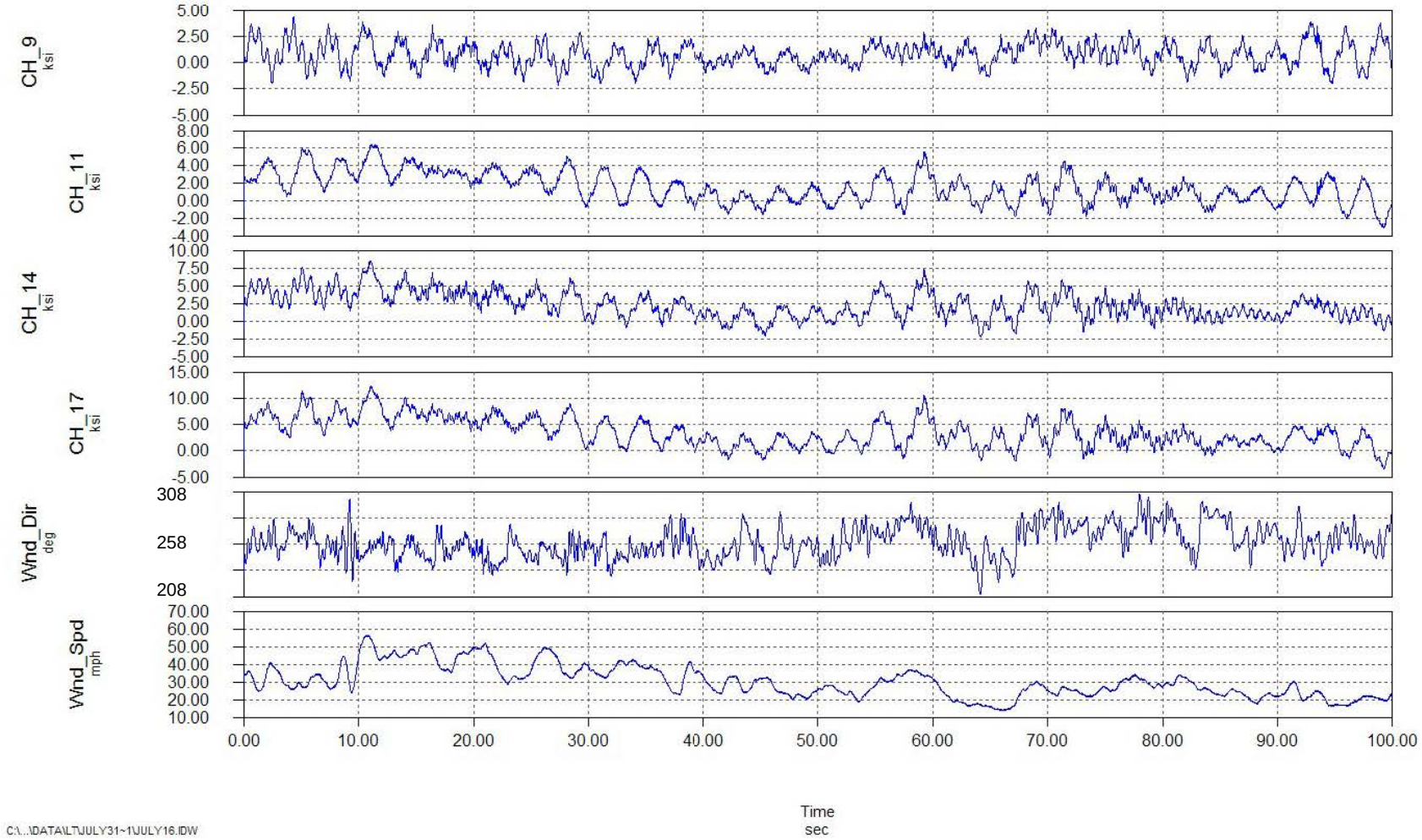

Figure 4.13 – High wind event – July 16, 2008 6:03 PM

4.2.3 Vortex Shedding

As with earlier phases of field testing, data were collected during periods in which the tower was excited by vortex shedding. Instances of excitation of the towers 2nd and 3rd modes of vibration were recorded.

Shown in Figure 4.14 is an example of vortex shedding in the third mode. At the time, the wind was out of the north west with a steady wind speed between 5 and 8 mph. This caused the tower to vibrate in its third mode at a frequency of approximately 3.4 Hz. This vibration occurred in a plane perpendicular to the prevailing wind. This is evident in the plot as the stress in strain gage CH_11 above the pole experiences oscillating stress since it lies near to this plane of vibration, where as CH_9 does not since it is not within the plane of vibration. These two strain gages are located 6 ft. above the base plate, and are 90 degrees apart on the tower.

It can be seen that this event lasted over 10 minutes (600 seconds), and that the stresses are relatively high at strain gage CH_17 at the bend point at the base of the jacket retrofit. The peak stress range is approximately 6 ksi at CH_17. Over 10 minutes at 3.4 Hz, this results in 2,040 cycles.

A second example of vortex shedding measured during the monitoring period is presented in Figure 4.15 which occurred on February 1, 2008 at 4:50 AM. In this case, a steady wind out of the north east at a speed of 3 to 5 mph excited the tower in its second mode of vibration, with a frequency of approximately 1.4 Hz. Again this vibration occurred in a plane perpendicular to the prevailing wind. This can be observed in the figure as the stress in strain gage CH_9 experiences oscillating stress due to vortex shedding whereas strain gage CH_11 does not. Note that this is opposite of the vortex shedding shown in Figure 4.14, since the wind direction is 90 degrees off.

This event only lasted approximately 5 minutes. At a frequency of 1.4 Hz, this resulted in a significantly lower approximate number of cycles of 420. A fairly high stress range was measured in strain gage CH_9 of approximately 5 ksi.

It can be seen that with this vortex shedding event, as the wind speed increased above approximately 3.5 mph, the amplitude of the vibration decreased since the wind speed was moving away from the critical lock-in wind speed.

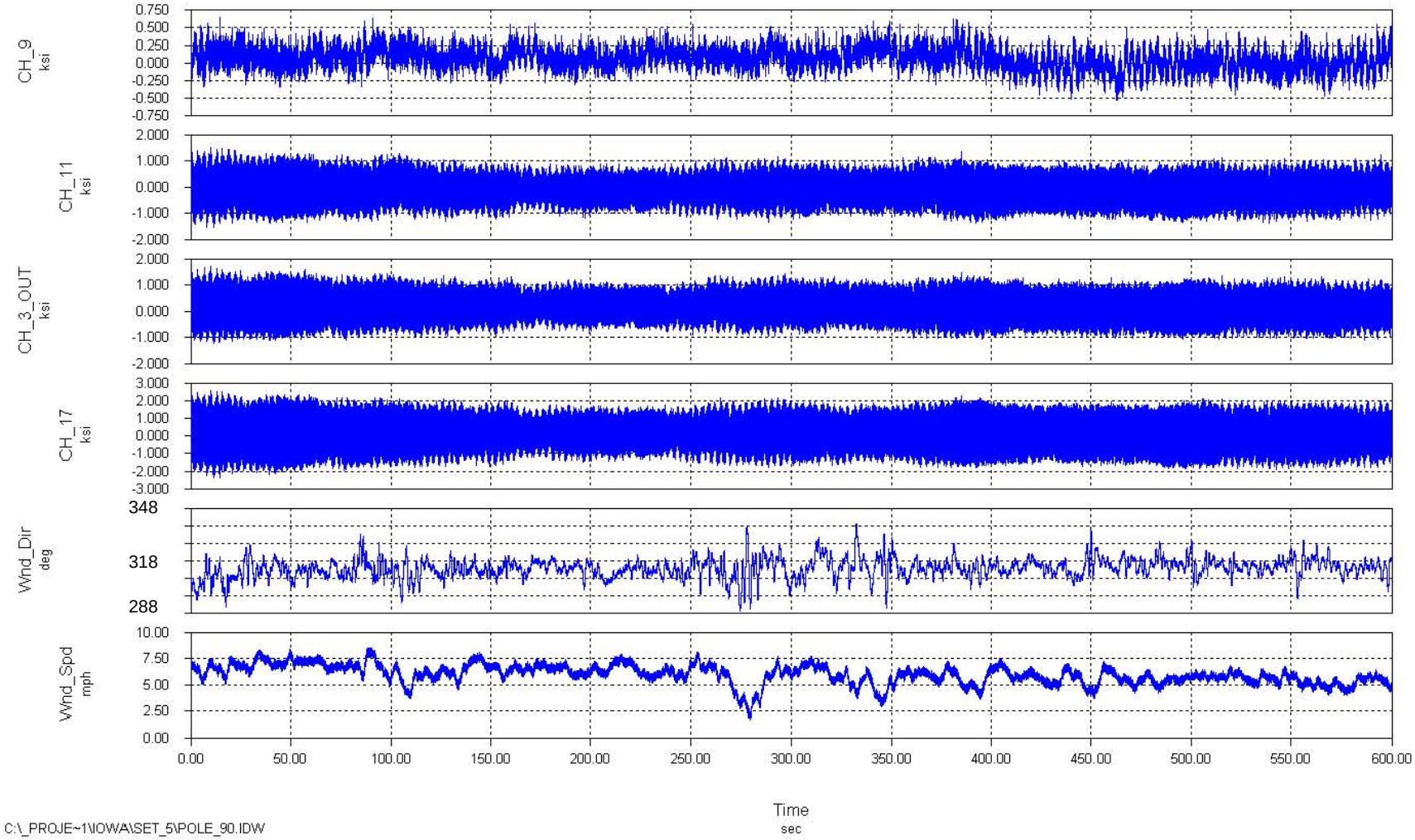

Figure 4.14 – 3rd mode vortex shedding (f = 3.4 Hz) – February 1, 2008 4:50 AM

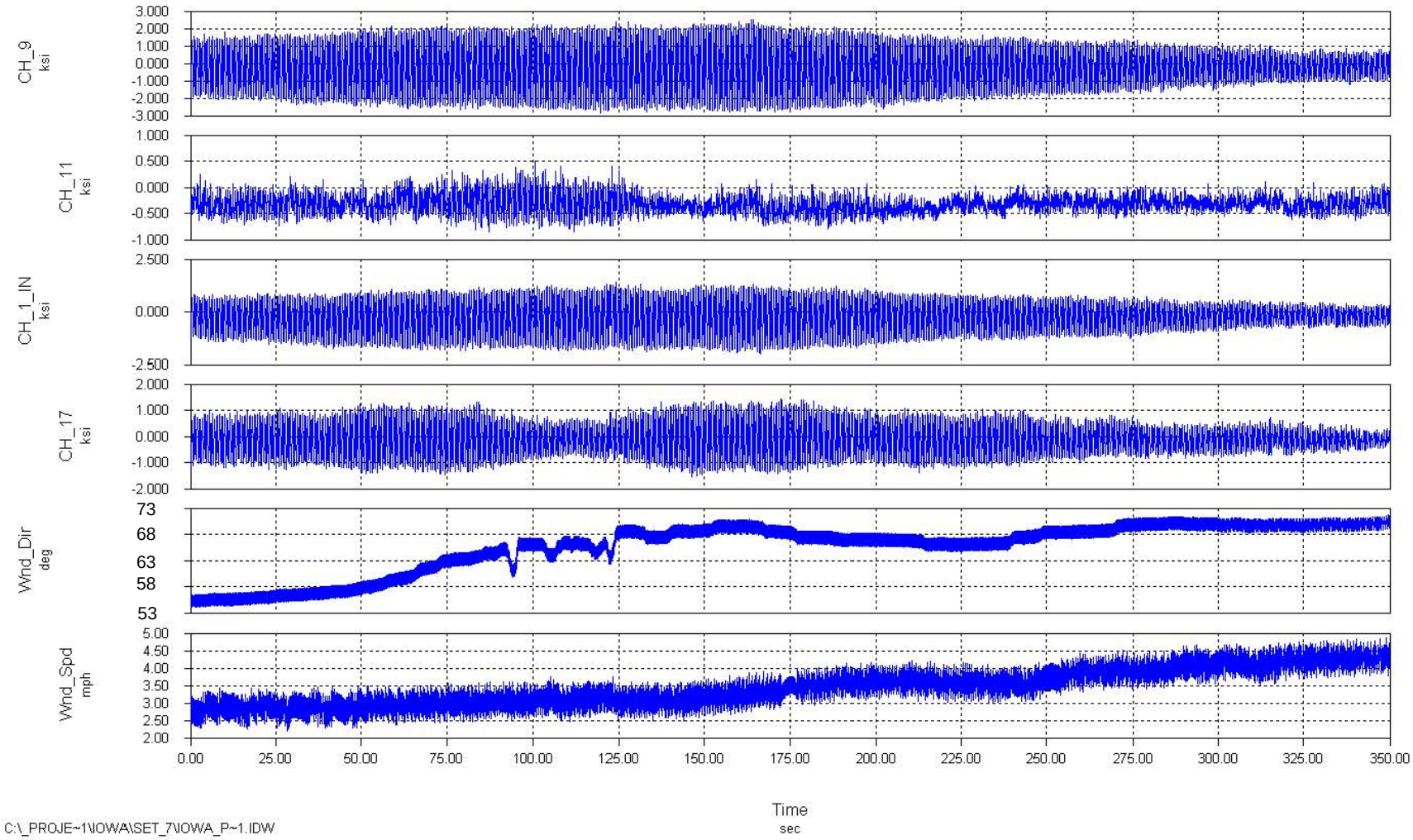

Figure 4.15 – 2nd mode vortex shedding (f = 1.4 Hz) – February 1, 2008 4:50 AM

5. Conclusions

The following conclusions can be drawn from the results presented above:

1. Static pull tests were performed on the high-mast tower in both the as-built and jacket-reinforced condition. The stresses in the tower were reduced by the presence of the jacket but not eliminated.
2. A total of 380 days of long-term data were collected. A large number of high-amplitude stress cycles were measured in the tower and reinforcing jacket. The highest observed stress ranges were found to be the result of buffeting from natural wind gusts. Peak stresses on the order of 25.8 ksi were measured at CH_17 (reinforcing jacket wall-to-base plate connection on the bend line). High stress ranges were also measured on the anchor rods (approximately 21.6 ksi at strain gage CH_14).
3. Vortex shedding in both the 2nd (frequency = 1.4 Hz) and 3rd modes (Frequency = 3.4 Hz) was observed during the long-term monitoring. The measured stress ranges during vortex shedding were lower than those caused by natural wind gusting, at approximately 5 ksi maximum. However, large numbers of cycles were accrued in a short time during vortex shedding.
4. The fatigue-life estimates indicate that finite fatigue life is expected at the following locations based on the results of the field monitoring and the results of the laboratory testing program:
    a. Existing tower-to-baseplate weld: *CH_1 - estimated life= 162 years; CH_3IN - estimated life =72 years*
    b. Reinforcing jacket wall-to-base plate connection: *CH_3OUT (at mid-face) – estimated life = 180 years; CH_17 (at bend) – estimated life = 30 years*
    c. Anchor Rod: *CH_14 – estimated life = 39 years*
5. Infinite fatigue is predicted on the existing tower above the reinforcing jacket, and near the top of the reinforcing jacket.
6. A two-lobed wind frequency distribution was measured at the tower, with predominant winds from 140 and 310 degrees.

6. References

1. Dexter, R.J., *Investigation of Cracking of High-mast Lighting Towers, Iowa Department of Transportation*, Ames, IA, September 2004.
2. Connor, R. J, Hodgson, I. C., *Field Instrumentation, Testing, and Long-term Monitoring of High-mast Lighting Towers in the State of Iowa*, Ames, IA, November 2006.
3. Miner, M.A., *Cumulative Damage in Fatigue*, Journal of Applied Mechanics, Vol. 1, No.1, Sept., 1945.
4. Downing S.D., Socie D.F., *Simple Rainflow Counting Algorithms*, International Journal of Fatigue, January 1982.
5. Fisher, J.W., Nussbaumer, A., Keating, P.B., and Yen, B.T., *Resistance of Welded Details Under Variable Amplitude Long-Life Fatigue Loading, NCHRP Report 354*, National Cooperative Highway Research Program, Washington, DC, 1993.
6. *Steel Structures – Material and Design*, Draft International Standard, International Organization for Standardization, 1994.
7. Schilling, C.G., *Variable Amplitude Load Fatigue, Task A - Literature Review: Volume I - Traffic Loading and Bridge Response*, Publication No. FHWA-RD-87-059, Federal Highway Administration, Washington, DC, July 1990.
8. Moses, F., Schilling, C.G., Raju, K.S., *Fatigue Evaluation Procedures for Steel Bridges, NCHRP Report 299*, National Cooperative Highway Research Program, Washington, DC, 1987.
9. Callahan G.L., Connor R.J., *Fatigue Performance of Multi-Sided High-Mast Lighting Towers and Bolted Retrofit Jackets*, Purdue University ,West Lafayette, Indiana, Oct. 2009

APPENDIX A

INSTRUMENTATION PLANS

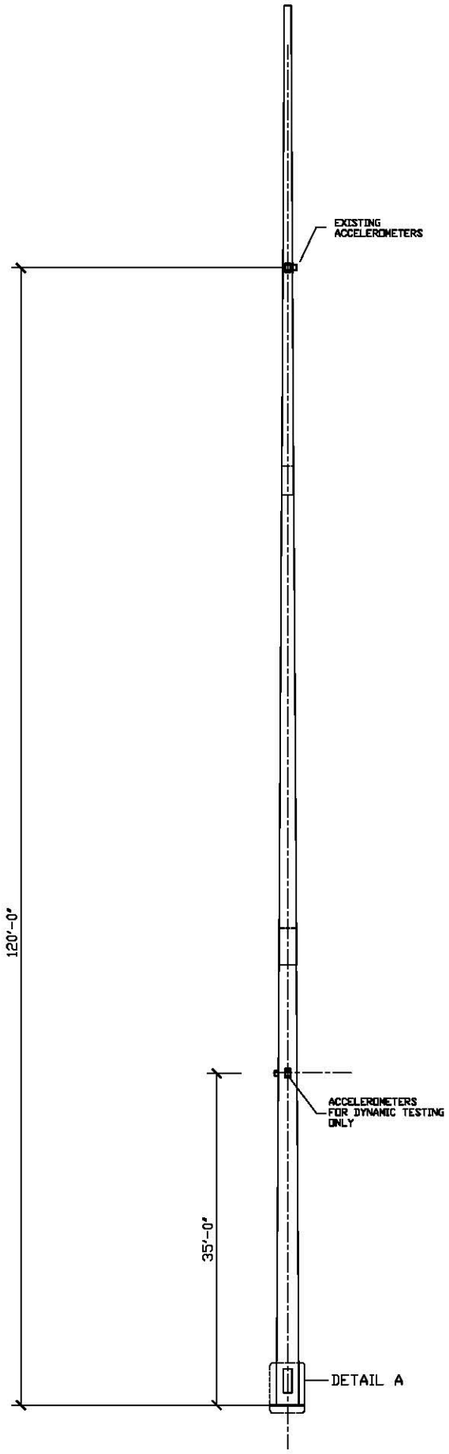

ELEVATION VIEW
SCALE: 1/16" = 1'-0"

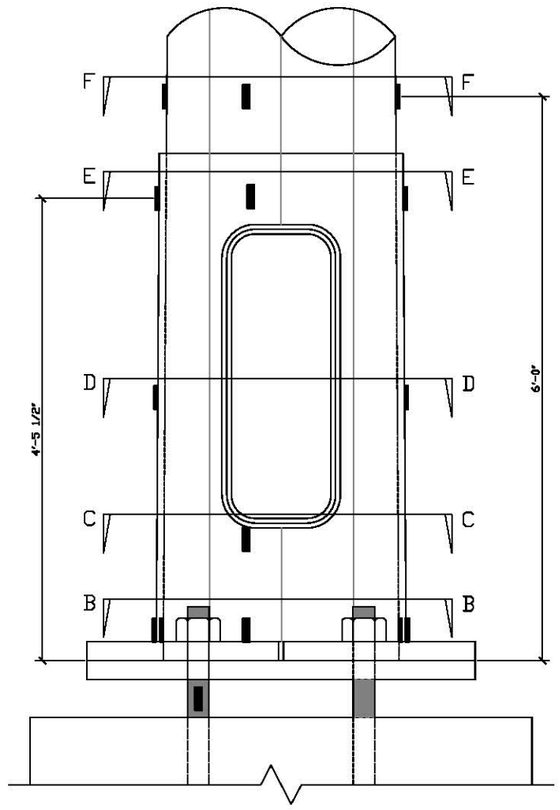

DETAIL A
SCALE: N.T.S.

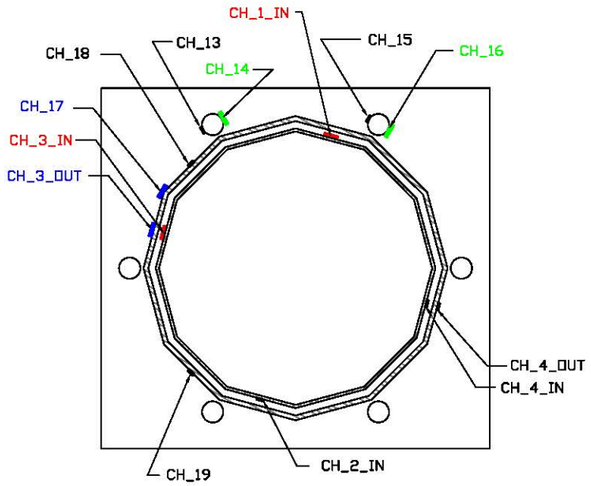

SECTION B-B
H = 0'-0" (@ WELD TOE)
SCALE: 3/4" = 1'-0"

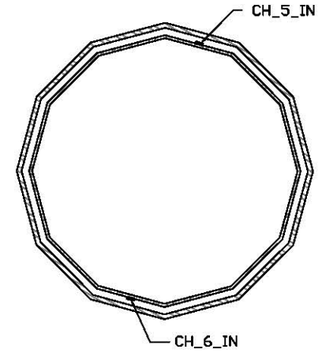

SECTION C-C
H = 12"
SCALE: 3/4" = 1'-0"

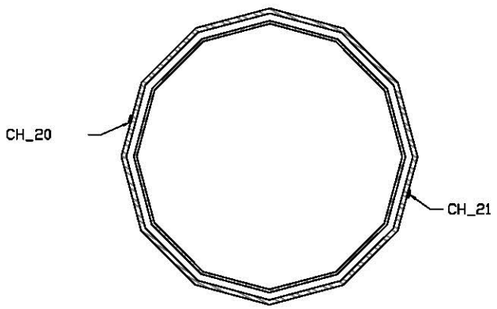

SECTION D-D
H = 1'-9 1/4"
SCALE: 3/4" = 1'-0"

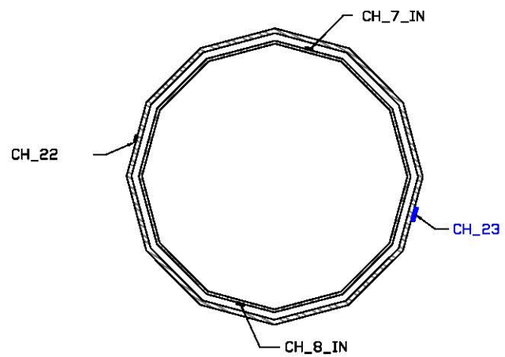

SECTION E-E
H = 4'-5 1/2"
SCALE: 3/4" = 1'-0"

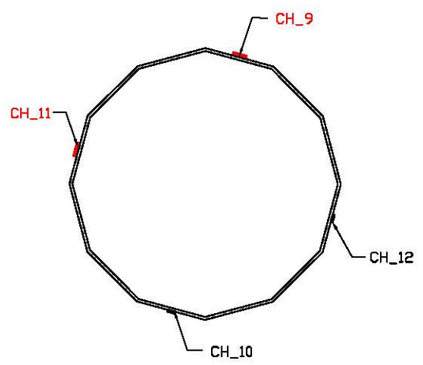

SECTION F-F
H = 6'-0"
SCALE: 3/4" = 6'-0"

ROBERT J. CONNOR & ASSOCIATES, LLC

PROJECT:

IOWA HIGH-MAST LIGHT POLE
PHASE 3 TESTING

SHEET NOTES:

1. ALL STRAIN GAGES TO BE MEASUREMENTS GROUP, INC. WELDABLE RESISTANCE GAGES TYPE LWK-08-W250B-350, U.O.N.

2. STRAIN GAGES INCLUDED IN THE LONG-TERM MONITORING PLAN ARE COLOR CODED AS FOLLOWS:

	NUMBER
= ORIGINAL SHELL	4
= JACKET	3
= ANCHOR RODS	2
TOTAL =	9

NO.	DESCRIPTION	DATE	BY
2	COLOR CODING	5/23/07	ICH
1	INITIAL SUBMITTAL	6/22/06	ICH

DESIGNED BY:	RJC/ICH
DRAWN BY:	ICH
CHECKED BY:	
SCALE:	AS SHOWN
DATE:	6/22/06
PROJECT NO.:	
SHEET TITLE:	

INSTRUMENTATION PLAN

SHEET NO.:

1 OF 1

APPENDIX B

Development of Stress-Range Histograms Used to Calculate Fatigue Damage

B.1 Stress-Range Histograms

The stress-range histogram data collected during the uncontrolled monitoring permitted the development of a random variable-amplitude stress-range spectrum for the selected strain gages. It has been shown that a variable-amplitude stress-range spectrum can be represented by an equivalent constant-amplitude stress range equal to the cube root of the mean cube (rmc) of all stress ranges (i.e., Miner's rule) [3] (i.e., $S_{reff} = [\Sigma\alpha_i S_{ri}^3]^{1/3}$).

During the long-term monitoring program, stress-range histograms were developed using the rainflow cycle counting method [4]. Although several other methods have been developed to convert a random-amplitude stress-range response into a stress-range histogram, the rainflow cycle counting method is widely used and accepted for use in most structures. During the long-term monitoring program, the rainflow analysis algorithm was programmed to ignore any stress range less than 0.50 ksi (18με). Hence, the "raw" histograms do not include these very small cycles. Such small cycles do not contribute to the overall fatigue damage of even the worst details and if included, can actually unconservatively skew the results, as will be discussed below. It is also worth mentioning, that in some testing environments, the validity of stress-range cycles less than this are often questionable due to electromechanical noise.

The effective stress range presented for each channel in the body of the report was calculated by ignoring all stress-range cycles obtained from the stress-range histograms that were less than predetermined limits. (*It should be noted that the limit described here should not be confused with the limit described above. The limit above (i.e., 0.50 ksi (18με)) refers to the threshold of the smallest amplitude cycle that was counted by the algorithm and not related to the cycles that were counted, but later ignored, to ensure an accurate fatigue life estimate, as will be discussed.*) For all welded steel details, a cut-off or threshold is appropriate and necessary, as will be discussed. The limits were typically about ¼ the constant amplitude fatigue limit for the respective detail. For example, for strain gages installed at details that are characterized as category C, with a CAFL of 10.0 ksi, the cutoff was set at 2.5 ksi. Hence, stress range cycles less than 2.5 ksi were ignored in the preparation of the stress-range histograms used to calculate the effective stress range and the number of cycles accumulated. The threshold was selected for two reasons.

Previous research has demonstrated that stress ranges less than about ¼ the CAFL have little effect on the cumulative damage at the detail [5]. It has also been demonstrated that as the number of random variable cycles of lower stress range levels are considered, the predicted cumulative damage provided by the calculated effective stress range becomes asymptotic to the applicable S-N curve. A similar approach of truncating cycles of low stress range is accepted by researchers and specifications throughout the world [6].

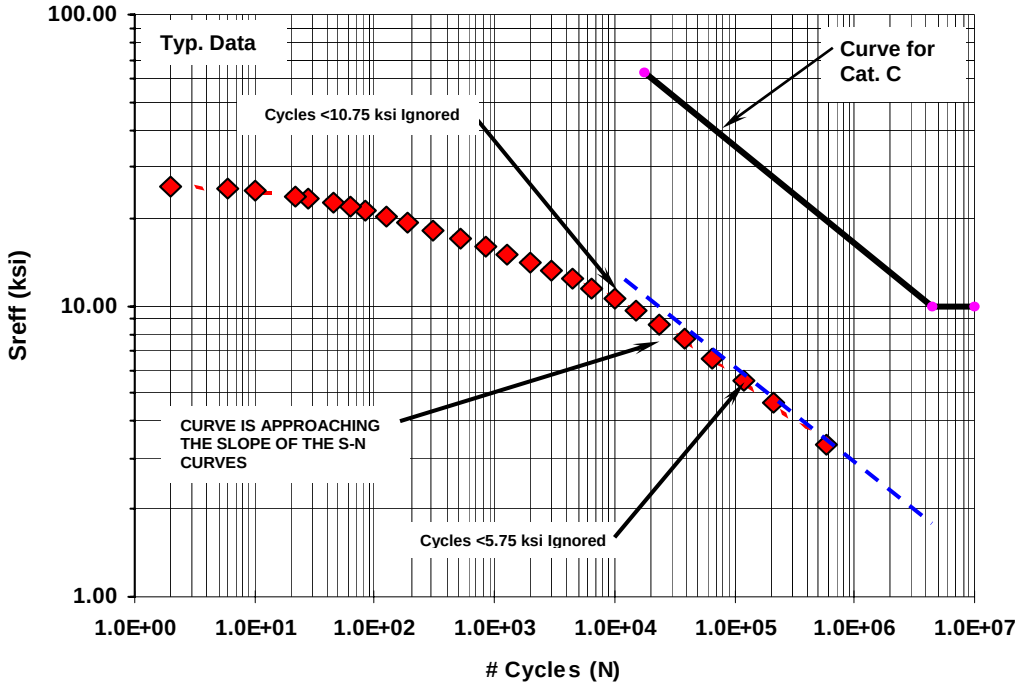

Figure B.1 – Effect of truncating cycles at different stress range cut off levels
(*Typical data from a stain gage at a fatigue sensitive detail*)

Figure B.1, shows the effect on the calculated effective stress range for several levels of truncation using typical field acquired long-term monitoring data collected from strain gage installed on a bridge. The data presented in Figure B.1 are also listed in Table B.1 showing the selected truncation level and its impact on the effective stress range.

As demonstrated by Figure B.1, as the truncation level decreases (from the lowest level), the effective stress range and corresponding number of cycles approaches the slope of the S-N curve for Category C, which is also plotted in Figure B.1 (i.e., a slope of –3 on a log-log plot). As long as the cut off level selected is consistent with the slope of the fatigue resistance curve, considering additional stress cycles at lower truncation levels does not improve the damage assessment and can therefore be ignored. As can be seen, using a truncation level as high as 10 ksi, the curve is nearly asymptotic to the slope of the S-N curves. Hence, an accurate prediction of the total fatigue life results.

It should also be noted that the load spectrum assumed in the AASHTO LRFD specifications for design was developed by only considering vehicles greater than about 20 kips [7]. Thus the AASHTO LRFD design also implicitly truncates and ignores stress cycles generated by lighter vehicles and vibration [8]. The observed frequency of stress cycles obtained from traffic counts is also consistent with the frequency of vehicles measured.

Cut Off (ksi)	Number Cycles > Cut Off Value	S_{reff} (ksi)
0.75	575,867	3.3
2.75	117,869	5.5
4.75	37,842	7.6
6.75	15,112	9.6
8.75	6,547	11.5
10.75	2,938	13.3
12.75	1,284	15.1
14.75	509	17.0
16.75	191	19.3
18.75	85	21.3
20.75	45	22.6
22.75	22	23.9
24.75	6	25.1
25.75	2	25.7

Table B.1 – Calculated effective stress ranges using different stress range cut off levels
Only every other data shown in Figure B.1 is shown for brevity

The maximum stress ranges listed in the tables developed in the body of this report were determined from the rainflow count. According to rainflow cycle counting procedures, the peak and valley that comprise the maximum stress range may not be the result of a single loading event and may in fact occur hours apart. In other words, an individual truck did not *necessarily* generate the maximum stress range shown in the tables. This is particularly true of distortion induced stresses that are subjected to reversals in stress due to eccentricity of the loading. In many cases, it was possible to identify this maximum stress range with a specific vehicle passage, but in other cases, the maximum rainflow stress range exceeded the maximum stress range from any individual vehicle. During the remote long-term monitoring program, the stress-range histograms were updated every ten minutes. Hence, the longest interval between nonconsecutive peaks and valleys is ten minutes.

B.2 Frequency of Exceedence of the CAFL

Based on experimental data, it has been found that when cycles in the variable amplitude spectrum exceed the CAFL often enough, then all stress cycles experienced by the structure can be considered to be damage-causing. This frequency of exceedence limit ranges between 0.01% and 0.05%. This corresponds to an occurrence of 1 in 10,000 or 1 in 2,000.

Research indicates that if this frequency limit is not exceeded, then it is reasonable to conclude that fatigue cracking would not be expected and infinite life can be assumed. However, if the limit is exceeded, the potential for fatigue cracking of the member exists and the fatigue life can be estimated by extending the given S-N curve. Obviously, this extension will only be required if the effective stress range (S_{Reff}) is less than the CAFL of the detail.

It should be noted that the limits are somewhat different for different details and the experimental data are limited. It is perhaps overly conservative to set the limit at 0.01% one for all details when conducting a fatigue evaluation. (*This is not an issue in the design of new structures.*) However, some owners may feel that 0.05% is too liberal and that a more conservative approach is best. Therefore, for the purposes of this study, a limit of 0.01% has been used.